

Sensor and Simulation Notes

Note 238

January 16, 1978

Performance Parameters Associated
with the FINES-Type Small EMP Simulators

Leih-Wei Chen
Dikewood Industries, Inc.

Carl E. Baum
Air Force Weapons Laboratory

CLEARED
FOR PUBLIC RELEASE
DL/PA 30 Dec 96

Abstract

Performance parameters associated with the FINES (Finite Intermediate Nuclear EMP Simulator) type of small simulator are studied in detail. FINES is a type of simulator which is intended to illuminate electrically small objects (such as antennas) or apertures on conducting surfaces by means of a locally placed simulator which produces the desired local surface current and/or charge densities. In general, there are four basic designing factors considered in this note: the response sensitivity of the simulated field to the input current or voltage, the uniformity of the simulated fields, the simulator's efficiency, and the simulator/test-object interaction; these can be used to characterize the performance of the FINES. Examples in the use of the performance parameters to quantify some important geometries pertinent to FINES published in the literature are given in two parts. First, for the canonical problems of unperturbed fields (i.e., simulators with all penetration being short-circuited and objects removed), one can define the relative field deviation as the deviation of the field within a desired working volume from the field measured at the center of the ground plane. Second, for the simulator/penetration interaction canonical problems, one considers the changes in the surface current and charge densities on the test object to be the important measure of the interaction. Other simulator/penetration interaction parameters, such as the change of the simulator impedance, the change of the impedance and the open-circuit voltage (or short-circuit current) at the terminals of antennas and the change of the polarizabilities of apertures, are also discussed.

Contents

<u>Section</u>		<u>Page</u>
I.	Introduction	3
II.	Performance Parameters of FINES	8
	A. Conversion Lengths	8
	B. Field Uniformity	11
	C. Figure of Merit and Efficiency	14
	D. Two-Dimensional FINES	17
	E. Interaction of Test Object with Simulator	20
III.	Canonical Problems for Unperturbed Fields	24
	A. Finite-Width Plate Above Ground Plane	24
	B. Cylindrical Plate Above Ground Plane	32
	C. Helmholtz Coils	41
	D. Maxwell Coils	49
IV.	Simulator/Object Interaction Canonical Problems	57
	A. Half Cylinder Between Infinite Large Plate and Ground Plane	57
	B. Half Cylinder Between a Finite-Width Plate and Ground Plane	61
	C. Prolate Hemispheroid Inside a Half Circular Loop	70
	D. Charged Filament Above an Earthed Slotted Sheet	76
	E. Large Plate Above Slotted Plane	80
V.	Summary	86
	References	92
	Acknowledgment	93

I. Introduction

The Finite Intermediate Nuclear EMP Simulator (FINES) is one type of the conceptually simple, inexpensive small electromagnetic pulse (EMP) simulators for testing the EMP hardness of military systems, in this case by individually exciting the electrically small penetrations. The FINES is intended to illuminate a portion of the system of interest (e.g., the deliberate antennas or the inadvertent apertures aboard an aeronautical system) to create a surface current \vec{J}_s and/or a surface charge ρ_s , locally over the penetration region which would be modeled from an incident nuclear EMP.

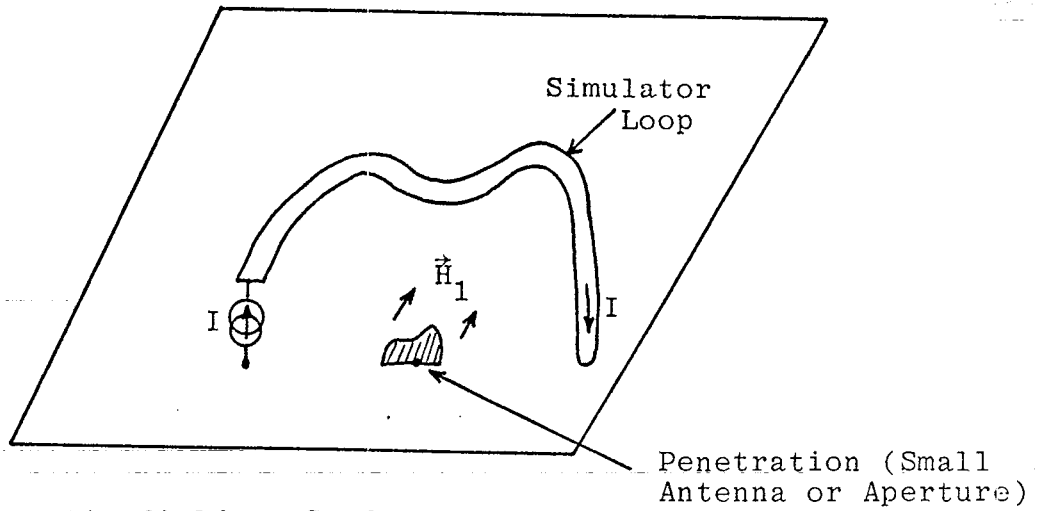
Since a FINES is appropriate for driving (electrically) small penetrations (small antennas and apertures) on high conducting surfaces of larger systems, a FINES can be designed which is also electrically small and produces approximately locally uniform electric and/or magnetic fields. Here, only the electric field normal to the system surface and the magnetic field parallel to the system surface are of interest. Thus, this type of simulator can be considered as a static (quasi-static) simulator and can also be termed zero-dimensional or point simulator which has been extensively discussed in reference 1. The basic limitation of a static

-
1. C. E. Baum, "EMP Simulators for Various Types of Nuclear EMP Environments: An Interim Categorization," Sensor and Simulation Note 151, 13 July 1972, AFWL. Also adapted for Special Joint Issue on the Nuclear Electromagnetic Pulse, IEEE Trans. Antennas and Propagation, January 1978, and IEEE Trans. Electromagnetic Compatibility, February 1978.

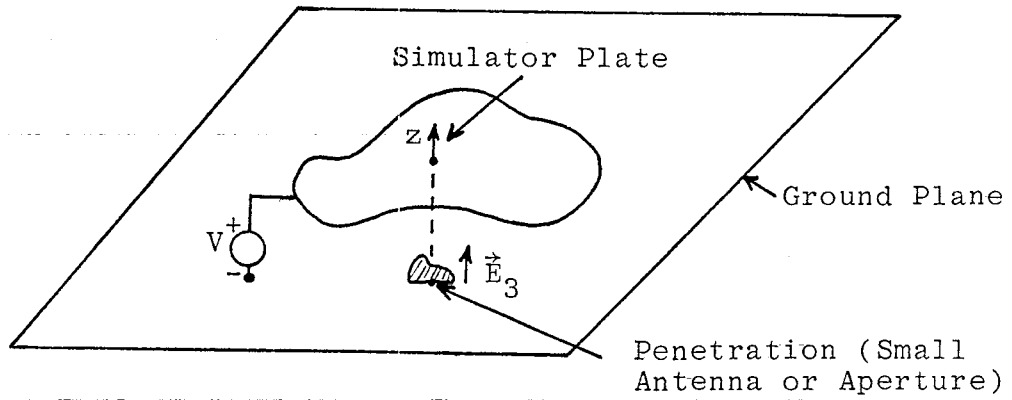
(quasi-static) simulator is that the frequencies of interest are sufficiently low or the corresponding radian wavelengths are large compared to the simulator structure so that the low-frequency or quasi-static form of the fields is applicable.

Generally, there are three kinds of designs for this class of simulators which are illustrated in figure 1. Figure 1(a) shows a loop type of simulator above the ground plane. The simulator is quasi-statically equivalent to a simple inductor driven by a constant current source and generates a uniform magnetic field near the (closed) penetration. Similarly, figure 1(b) shows a voltage source connected between the simulator plate and the ground plane; the plate and ground plane can be simply characterized by a capacitor driven by a constant voltage source to generate a uniform electric field near the (closed) penetration. Figure 1(c) shows a combined version of the electric and magnetic types of simulator described by figures 1(a) and 1(b); note that a maximum of two components of the magnetic field can be combined with one of the electric field. The conversion of input sources to fields of the FINES is just opposite to the concept of an electrically small EMP sensor (to be seen as an electric or a magnetic dipole) which induces an open-circuit voltage or a short-circuit current at its terminals by picking up the local electric or magnetic fields incident to the sensor; this is a form of reciprocity (ref. 2).

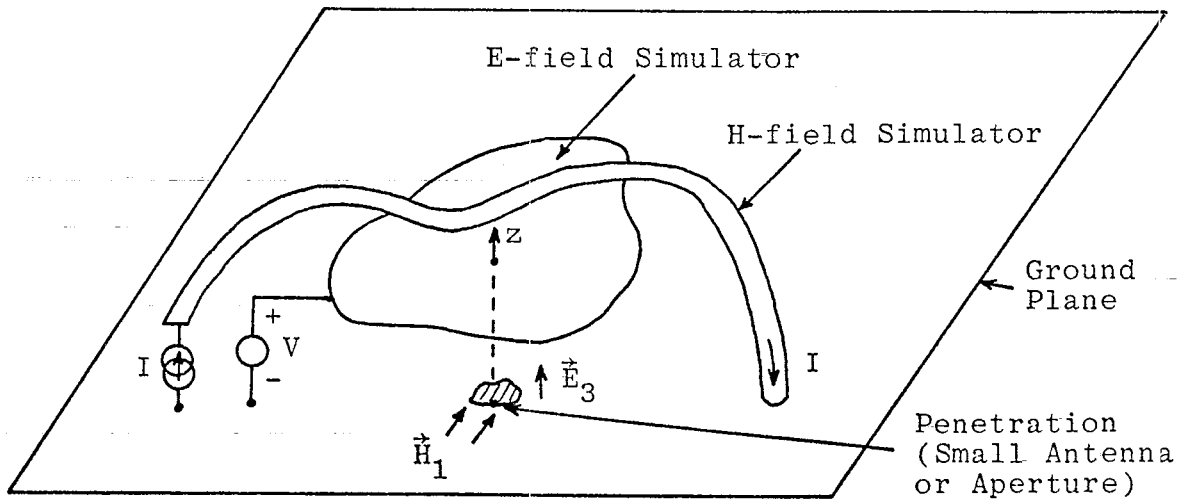
-
2. C. E. Baum, E. L. Breen, J. C. Giles, J. O'Neill, and G. D. Sower, "Sensors for Electromagnetic Pulse Measurement Both Inside and Away from Nuclear Source Regions," Special Joint Issue on Nuclear Electromagnetic Pulse, IEEE Trans. Antennas and Propagation, January 1978, and IEEE Trans. Electromagnetic Compatibility, February 1978.



a. Magnetic-field or Surface-Current-Density Type of FINES



b. Electric-field or Surface-Charge-Density Type of FINES



c. Combined Electric and Magnetic Fields (or Charge and Current Densities) Type of FINES

Figure 1. Configurations of the FINES-type Simulators

In designing a proper FINES, one studies the conversion of the input sources V and I by an appropriate constant to ρ_s and \vec{J}_s , respectively, on the surface of the system with the penetration short-circuited (i.e., a smooth conducting surface). From the study one predicts the simulator performance qualities which include the field spatial uniformity, the useful energy (efficiency), etc. However, in practice the simulator will be placed near the penetration and the interaction between them should also be taken into account.

In general, there are four basic factors that can be used to characterize the performance of FINES:

(1) The response sensitivity of the simulated fields to the input current (or voltage).

(2) The uniformity of the simulated field in the neighborhood of the test object with the test object removed (or surface short-circuited, i.e., a smooth conducting surface).

(3) The simulator's figures of merit and efficiencies relating fields and field energies to voltage or current and energy delivered to the simulator.

(4) The interaction between the simulator and the penetration being excited.

In this report we will define these performance parameters and utilize them to quantify various canonical problems via the review of the previous work published in the literature (particularly, Sensor and Simulation Notes). Our analysis in this report is limited to the quasi-static solution, i.e., all radian

wavelengths of interest are sufficiently large compared to the simulator dimensions. Other important considerations related to the design of the FINES, such as the type of input sources and the feeding network to be used, will not be covered here. Future studies should be extended to these areas.

II. Performance Parameters of FINES

A. Conversion Lengths

The conversion lengths are used to quantify the simulator's sensitivity of the simulated fields to the input sources. In general, there are three types of simulators according to the fields they generate, the E-field, the H-field and the combined-fields simulators. The fields which they generate can be expressed in terms of the conversion lengths ℓ_{c_m} defined by

H-Field Simulator

$$\vec{H}_0 = \vec{i}_m \ell_{c_m}^{-1} I_m, \quad m = 1 \text{ or } 2 \quad (1)$$

E-Field Simulator

$$\vec{E}_0 = \vec{i}_3 \ell_{c_3}^{-1} V, \quad m = 3$$

Here, \vec{E}_0 and \vec{H}_0 are the fields measured at the center of the ground plane where a test object or aperture is to be placed, V and I_m are the voltage and current sources applied to the simulator, and \vec{i}_m ($m=1,2,3$) denote mutually orthogonal unit-vectors tangential and normal to the ground plane in a right-handed system (see fig. 2). Alternatively, we can express unit-vectors \vec{i}_1, \vec{i}_2 (or $\vec{i}_{T_1}, \vec{i}_{T_2}$) as orthogonal unit vectors tangential to the ground surface S , and \vec{i}_3 (or \vec{i}_S) as unit outward pointing vector normal to the ground surface S . Their orthogonal relations are

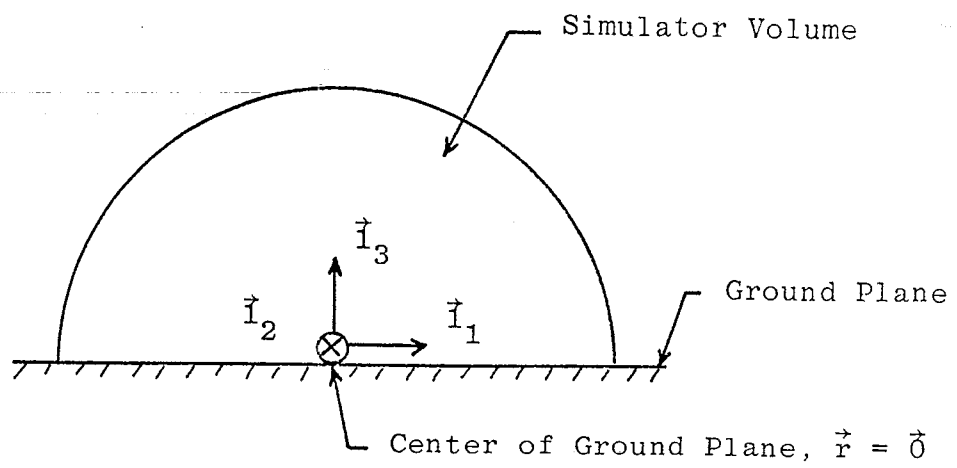


Figure 1. Unit Vectors for FINES Description

$$\begin{aligned} \hat{i}_1 \times \hat{i}_2 &= \hat{i}_3, \quad \hat{i}_2 \times \hat{i}_3 = \hat{i}_1, \quad \hat{i}_3 \times \hat{i}_1 = \hat{i}_2 \\ \hat{i}_1 \cdot \hat{i}_2 &= 0, \quad \hat{i}_2 \cdot \hat{i}_3 = 0, \quad \hat{i}_3 \cdot \hat{i}_1 = 0 \end{aligned} \quad (2)$$

Combined Fields Simulator

This type of simulator is able to generate the E-field and H-field, either an individual component or in various combinations, and can be driven by a single source or a set of independent sources. If the interaction between the different desired field components of the simulator is negligibly small (by symmetry in the design) and all radian wavelengths of interest are sufficiently large compared to the simulator dimensions (quasi-static approximation), then we are able to consider that the E-field is generated via a constant voltage source and the H-field is generated via a constant current source. Under these restrictions, the same relations given by (1) can be used to quantify the sensitivity of the combined fields type of FINES simulator.

B. Field Uniformity

To describe the field quality of a simulator, we can define a maximum allowable volume, namely the working volume, inside which the field is uniform everywhere within a certain percentage deviation from the field at the center of the ground plane. For convenience, a hemisphere with a radius a_w (fig. 3) is chosen to be an E-field simulator's working volume with volume V_w as

$$V_w = \frac{2}{3} \pi a_w^3 \quad (3)$$

The maximum allowable radius a_w for a given electric field variation is determined by the inequality

$$\frac{|\vec{E}(\vec{r}) - \vec{E}_0|}{|\vec{E}_0|} \leq \Delta \text{ for all } \vec{r} \in V_w \text{ (} r \equiv |\vec{r}| < a_w \text{)} \quad (4)$$

$$\vec{E}_0 \equiv \vec{E}(\vec{0})$$

where Δ denotes the relative deviation from the field at the center of the ground plane and is less than 1. Ideally, for a simulator of good field quality, Δ is much less than 1 (i.e., $\Delta \ll 1$) for a given working volume radius a_w .

In addition, by examining the derivatives of the field at the center of the ground plane and by making more higher order derivatives vanish, sometimes we can obtain an optimal field uniformity if some geometrical constraints to the simulator are given.

In general, the geometrical symmetry of a simulator can be used to make at least the first derivative (usually the derivatives

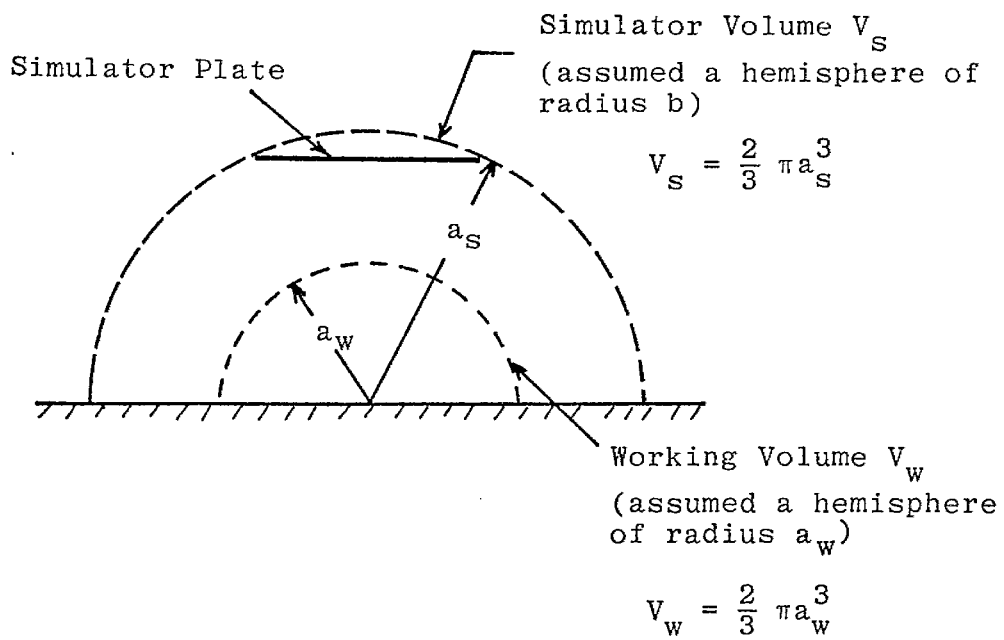


Figure 3. Working Volume and Simulator Volume

of all odd orders) of the field components (with respect to x, y, and z) vanish at the center ($\vec{r} = \vec{0}$) which is by definition on the ground plane (an equivalent symmetry plane by image theory).

To complement the working-volume concept we can define a simulator volume as a hemisphere of radius a_s centered on $\vec{r} = \vec{0}$ (with surface $r \equiv |\vec{r}| = a_s$) with volume

$$V_s = \frac{2}{3} \pi a_s^3 \quad (5)$$

Here, a_s is defined as the minimum r such that V_s contains at least the basic simulator conductors, dielectrics, etc., (perhaps excluding peripheral hardware such as connectors, transformers, etc.). For example, a_s is found to be the radius of a sphere circumscribed to the actual simulator plate as shown in figure 3.

If the penetration (e.g., a long slit) to be excited has much larger longitudinal dimension than its transverse dimensions and if the FINES has a two-dimensional configuration such as a plate-ground-plane transmission-line simulator, it is more convenient to use the hemi-cylinders to characterize the simulator and working volumes instead of using the hemispheres. Therefore, a_s and a_w can be denoted as the radii of the cylindrical simulator and working volumes, respectively.

C. Figure of Merit and Efficiency

One possible definition of the figure of merit of a simulator can be constructed by maximizing the working-volume radius to conversion-length ratio

$$\xi_{\ell} \equiv \frac{a_w}{\ell c_m}, \quad m = 1, 2, 3 \quad (6)$$

where ξ_{ℓ} is a function of the field deviation Δ . For a given allowable field deviation, one would like the simulator to have a large working volume but a small conversion length.

Another definition of the figure of merit based on energy considerations can be expressed in the form of the simulator's efficiency

$$\xi \equiv \frac{\text{ideal total energy enclosed within the working volume } (U_w)}{\text{total energy delivered to the simulator } (U_{in})} \quad (7)$$

If the field \vec{E} or \vec{H} is uniform inside a simulator working volume V_w , the total energy inside the volume is given by

$$U_w = \begin{cases} \frac{1}{2} \mu_0 |\vec{H}_0|^2 V_w & \text{for the H-field simulator} \\ \frac{1}{2} \epsilon_0 |\vec{E}_0|^2 V_w & \text{for the E-field simulator} \end{cases} \quad (8)$$

ϵ_0 = permittivity of free space

μ_0 = permeability of free space

where \vec{E}_0 and \vec{H}_0 are the field measured at the center of the ground plane enclosed by the working volume. This is taken as a

definition of the ideal working-volume energy (i.e., fields are assumed uniform throughout V_w).

If the E-field simulator is assumed to be open-circuited (a capacitor) and the H-field simulator is assumed to be short-circuited (an inductor), we define the input energy by

$$U_{in} = \begin{cases} \frac{1}{2} LI^2 & \text{for the H-field simulator} \\ \frac{1}{2} CV^2 & \text{for the E-field simulator} \end{cases} \quad (9)$$

By using the linearity relation between the input source and the simulated fields given by (1), we can rewrite the input energy as (quasi-static assumption)

$$U_{in} = \begin{cases} \frac{1}{2} L \ell_{c_m}^2 |\vec{H}_0|^2, & m = 1,2 \text{ for the H-field simulator} \\ \frac{1}{2} C \ell_{c_3}^2 |\vec{E}_0|^2, & m = 3 \text{ for the E-field simulator} \end{cases} \quad (10)$$

Inserting (8) and (10) into (7), the efficiency of such a simulator can be expressed as

H-field Simulator ($m = 1,2$):

$$\xi_h = \frac{\frac{1}{2} \mu_0 |\vec{H}_0|^2 V_w}{\frac{1}{2} L |\vec{H}_0|^2 \ell_{c_m}^2} = \frac{\mu_0 V_w}{L \ell_{c_m}^2}$$

E-field Simulator (m = 3): (11)

$$\xi_e = \frac{\frac{1}{2} \epsilon_0 |\vec{E}_0|^2 V_w}{\frac{1}{2} C |\vec{E}_0|^2 \ell_{c_3}^2} = \frac{\epsilon_0 V_w}{C \ell_{c_3}^2}$$

From this we define an equivalent volume V_{eq} for the simulator from

$$\xi_h \equiv \frac{V_w}{V_{eq}}, \quad \xi_e \equiv \frac{V_w}{V_{eq}} \quad (12)$$

which implies a definition

$$V_{eq} \equiv \begin{cases} \frac{L}{\mu_0} \ell_{c_m}^2, & m = 1, 2 \text{ for the H-field simulator} \\ \frac{C}{\epsilon_0} \ell_{c_3}^2, & \text{for the E-field simulator} \end{cases} \quad (13)$$

This energy-efficiency figure of merit ξ_h or ξ_e is relatable to the working-volume radius to conversion-length figure of merit ξ_ℓ in (6) as

H-field Simulator (m = 1, 2):

$$\xi_h = \frac{\mu_0}{L} \frac{2\pi}{3} \frac{a_w^3}{\ell_{c_m}^2} = \frac{2\pi}{3} \frac{\mu_0}{L} a_w \xi_\ell^2 = \frac{2\pi}{3} \frac{\mu_0}{L} \ell_{c_m} \xi_\ell^3 \quad (14)$$

E-field Simulator (m = 3):

$$\xi_e = \frac{\epsilon_0}{C} \frac{2\pi}{3} \frac{a_w^3}{\ell_{c_3}^2} = \frac{2\pi}{3} \frac{\epsilon_0}{C} a_w \xi_\ell^2 = \frac{2\pi}{3} \frac{\epsilon_0}{C} \ell_{c_3} \xi_\ell^3 \quad (15)$$

Note that expressions (14) and (15) are derived by assuming that the working volume is a hemisphere of radius a_w .

D. Two-Dimensional FINES

For simulators with two-dimensional configurations (e.g., a plate-ground-plane transmission-line simulator), their inductance and capacitance are more conveniently expressed in per-unit-length form and thus expressions (13), (14), and (15) can be modified as follows.

For the H-field simulator, the equivalent volume is given by

$$\begin{aligned} V_{eq} &= \frac{L' \ell}{\mu_0} \ell_{c_1}^2 = \frac{Z_c}{\mu_0} \frac{\ell}{c} \ell_{c_1}^2 \\ &= f_g \ell \ell_{c_1}^2 \quad \text{for } m = 1 \text{ (} m = 2 \text{ being irrelevant)} \end{aligned} \quad (16)$$

$$c = \frac{1}{\sqrt{\mu_0 \epsilon_0}} = \text{speed of light}$$

$$Z_0 = \sqrt{\frac{\mu_0}{\epsilon_0}} = \text{wave impedance of free space}$$

where L' denotes the inductance per unit length, ℓ is the length of the simulator, and Z_c is the transmission-line characteristic impedance. Here, the simulator's geometrical impedance factor is defined by

$$f_g = \frac{\text{simulator's characteristic impedance } Z_c}{\text{medium (free space) impedance } Z_0} \quad (17)$$

The simulator's efficiency ξ_h can be written as

$$\xi_h = \frac{V_w}{V_{eq}} = \frac{2\pi a_w^3/3}{\ell \ell_{c_1}^2 f_g}$$

$$\frac{\ell}{a_w} \xi_h = \frac{2\pi a_w^2/3}{\ell_{c1}^2 f_g} \quad (18)$$

Note that ξ_h is normalized to a_w because a_w is the given dimension of the desired working volume.

Similarly, for the E-field simulators V_{eq} is expressed as

$$\begin{aligned} V_{eq} &= \frac{C' \ell}{\epsilon_0} \ell_{c3}^2 = \frac{1}{\epsilon_0 Z_c} \frac{\ell}{c} \ell_{c3}^2 \\ &= \frac{1}{f_g} \ell \ell_{c3}^2 \end{aligned} \quad (19)$$

where C' is the capacitance per unit length of the simulator.

The efficiency ξ_e is given by

$$\begin{aligned} \xi_e &= \frac{V_w}{V_{eq}} = \frac{2\pi a_w^3/3}{\ell \ell_{c3}^2 / f_g} \\ \frac{\ell}{a_w} \xi_e &= \frac{2\pi a_w^2/3}{\ell_{c3}^2 / f_g} \end{aligned} \quad (20)$$

Note that for a two-dimensional geometry (as above) the efficiency ξ_e is inversely proportional to the length of the simulator (as expected).

The conversion lengths ℓ_{c1} and ℓ_{c3} and simulator's efficiencies ξ_h and ξ_e of the H-field and E-field, respectively, for the two-dimensional simulator (TEM) are related to each other. From (1) the conversion lengths can be expressed in terms of the ratio of the input current and voltage to the simulated magnetic and electric field, respectively, as

$$l_{c_1} = \frac{I}{H_0} \quad (21)$$

$$l_{c_3} = \frac{V}{E_0} \quad (22)$$

By taking the ratio of (22) to (21), the geometrical impedance factor f_g is given by

$$\frac{V}{I} = Z_c = f_g Z_0 = \frac{E_0 l_{c_3}}{H_0 l_{c_1}} = Z_0 \frac{l_{c_3}}{l_{c_1}} \quad (23)$$

$$f_g = \frac{l_{c_3}}{l_{c_1}}$$

Thus, the expression (16) or (19) of the equivalent volume V_{eq} can be rewritten as

$$V_{eq} = l l_{c_1} l_{c_3} \quad (24)$$

Now substituting (23) for f_g back into the efficiency expressions (18) and (20), we obtain

$$\xi_h = \xi_e = \frac{2\pi a_w^3/3}{l l_{c_1} l_{c_3}} = \xi \quad (25)$$

$$\frac{l}{a_w} \xi = \frac{2\pi a_w^2}{3 l_{c_1} l_{c_3}}$$

E. Interaction of Test Object with Simulator

One of the more important simulator design questions is what one refers to as the simulator/object interaction. The object inside a simulator scatters fields which in turn are re-scattered from the simulator back to the test object, thereby changing the ultimate response of the test object. This process can be viewed as a change in the kernel (Green's function) of an appropriate integral equation for currents or charges on the test object or as an infinite multiple-scattering sequence.

We would like to quantify the effects of this process so that the resulting errors can be kept down to an acceptable limit by making the simulator structure sufficiently distantly spaced from the test object. For the present discussion, changes in surface current and charge densities (for H-field and E-field types, respectively) on the test object will be considered as the important measure of this error. However, depending on the specific shape and function of the test object, there are other parameters one might consider as well. Examples are inductance or capacitance changes in the test object and mutual inductances and capacitances to the simulator where appropriate for certain types of antennas; for such antennas one might also consider changes in open-circuit voltage and/or short-circuit current at their terminals. For apertures on the other hand, one might consider changes in the equivalent dipole moments (magnetic ($m = 1,2$) and electric ($m = 3$) as subscripts) due to the simulator/aperture interaction mechanism.

Other kinds of changes associated with this effect are also observable at the driving terminals of the simulator. Specifically, the inductance of an H-field type and the capacitance of an E-field type of simulator will be changed by the presence of the object, and so parameters such as these should be considered.

a. H-field Simulator/Object Interaction

The parameters used to quantify the interaction between the H-field simulator and the object are:

(1) $\frac{\Delta L}{L}$ as a function of the object and simulator geometry parameters. Here, L is the inductance of the simulator and ΔL is the change in simulator's inductance associated with the presence of the object (or aperture).

(2) $\frac{|\Delta \vec{J}_s(\vec{r})|}{|\vec{J}_s(\vec{r})|}$ as a function of the object and simulator geometry parameters. Here, $\vec{J}_s(\vec{r})$ is the surface current density along the conducting object in the simulator (or perhaps some equivalent current in an aperture) and $\Delta \vec{J}_s(\vec{r})$ is the change of the surface current density on the object surface inside a simulator compared to the "free field" solution. By "free field" solution, we mean that a $\vec{J}_{s_f}(\vec{r})$ is found from $\vec{H}_f(\vec{r})$ defined as the actual field (for a given I) in the simulator with object removed (i.e., ground plane shorted), and using $\vec{H}_f(\vec{r})$ as an incident magnetic field on the object, but with the simulator removed (i.e., no interaction of the simulator with the scattered fields). Hence we have

$$\Delta \vec{J}_s(\vec{r}) \equiv \vec{J}_{s_f}(\vec{r}) - \vec{J}_s(\vec{r}) \quad (26)$$

Define

$$\Delta_{SO} \equiv \max_{\vec{r} \in V_w} \frac{|\Delta \vec{J}_s(\vec{r})|}{|\vec{J}_{sf}(\vec{r})|} \quad (27)$$

with the object within V_w . By constraining Δ_{SO} as some dimensionless number (ideally $\Delta_{SO} \ll 1$) one can find a maximum allowable object radius for given simulator dimensional parameters

(a_s, ℓ_{c_m} ($m = 1, 2$), etc.), for which a desired Δ_{SO} is achieved.

b. E-field Simulator/Object Interaction

Similarly, the important parameters which can be used to quantify the extent of the interaction between the E-field simulator and the object are

(1) $\frac{\Delta C}{C}$ as a function of the object and simulator

geometry parameters. Here, C denotes the capacitance of the simulator without the presence of the object and ΔC is the change in simulator's capacitance with the presence of object (or aperture).

(2) $\frac{\Delta \rho_s(\vec{r})}{\rho_s(\vec{r})}$ as a function of the object and simulator

geometry parameters. Here, $\rho_s(\vec{r})$ is the surface charge density along the conducting object in the simulator (or perhaps some equivalent charge density in an aperture) and $\Delta \rho_s(\vec{r})$ is the change of the surface charge density induced on the object surface inside a simulator compared to the "free field" solution. Again, the "free field" solution is found to be the surface charge density $\rho_{sf}(\vec{r})$ by using $\vec{E}_f(\vec{r})$ as an incident electric field on the object with the simulator removed (i.e., no interaction of the simulator with the scattered field). $\vec{E}_f(\vec{r})$ is the actual field (for a given V) in the simulator with the object removed (i.e., ground plane shorted). Hence we have

$$\Delta\rho_s(\vec{r}) \equiv \rho_{s_f}(\vec{r}) - \rho_s(\vec{r}) \quad (28)$$

Define for the object within V_w

$$\Delta_{so} \equiv \max_{\vec{r} \in V_w} \frac{|\Delta\rho_s(\vec{r})|}{|\rho_{s_f}(\vec{r})|} \quad (29)$$

By constraining Δ_{so} as some dimensionless number (ideally $\Delta_{so} \ll 1$), one can find a maximum allowable object radius (it may be the radius of a sphere circumscribing the actual object surface, i.e., the worst case is considered) for given simulator dimensional parameters (a_s, ℓ_{c_3} , etc.), for which a desired Δ_{so} is achieved.

III. Canonical Problems for Unperturbed Fields

A. Finite-Width Plate Above Ground Plane

The geometrical impedance factor f_g of a finite-width plate above ground plane (fig. 4) is given by

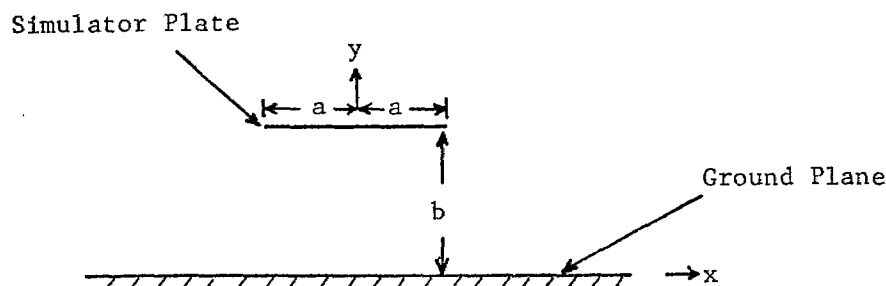


Figure 4. Configuration of Finite-Width Plate Simulator

$$f_g = \frac{1}{2} \frac{K(m_1)}{K(m)} \quad , \quad m_1 = 1 - m \quad (30)$$

where m is related to the simulator's width-to-height ratio (a/b) from equations:

$$\frac{a}{b} = \frac{2}{\pi} [K(m) E(\phi_0/m) - E(m) F(\phi_0/m)]$$

$$\sin \phi_0 = \left[\frac{1}{m} \left(1 - \frac{E(m)}{K(m)} \right) \right]^{\frac{1}{2}} \quad (31)$$

$F(\phi_0/m)$ = incomplete elliptic integral of the first kind

$E(\phi_0/m)$ = incomplete elliptic integral of the second kind

$K(m)$ = complete elliptic integral of the first kind

$E(m)$ = complete elliptic integral of the second kind

The numerical values of f_g are tabulated in table 1 (ref. 3).

Note that the geometrical impedance factor f_g of a plate above the ground plane is equal to one half the value of a two-parallel-plate transmission line.

The conversion length ℓ_{c_1} or ℓ_{c_3} can be obtained by

$$\ell_{c_3}^{-1} b = \frac{\pi}{2K(m_1)} E(m) = E_{y_{rel}}(0,0) = (\ell_{c_1} f_g)^{-1} b \quad (32)$$

where $E_{y_{rel}}(x,y)$ is the imaginary component of the complex electric field $E_{rel}(z)$ defined by

$$E_{rel}(z) = E_{x_{rel}}(x,y) - j E_{y_{rel}}(x,y) \quad (33)$$

$z = x + jy =$ complex coordinates

The numerical values of ℓ_{c_3}/b can be found in table 1.

The complex electric field of a finite-sized plate above the ground plane can be expressed as

$$E_{rel}(z) \equiv E_{x_{rel}}(x,y) - j E_{y_{rel}}(x,z) = \frac{b}{K(m_1)} \frac{dw}{dz} \quad (34)$$

$$\frac{z}{b} \equiv \zeta = \frac{2j}{\pi} \{K(m) E(w/m_1) + w[E(m) - K(m)]\}$$

-
3. C. E. Baum, D. V. Giri, and R. D. Gonzalez, "Electromagnetic Field Distribution of the TEM Mode in a Symmetrical Two-Parallel-Plate Transmission Line," Sensor and Simulation Note 219, 1 April 1976.

Table 1

GEOMETRICAL IMPEDANCE, CONVERSION LENGTH AND EQUIVALENT VOLUME
FOR THE FINITE-WIDTH-PLATE SIMULATOR

b/a	$2Z_c$ (ohms)	f_g	$k_{c3} b^{-1}$	$V_{eq} (kb^2)^{-1} =$ $(k_{c3} b^{-1})^2 f_g^{-1}$
0.16670	50.240	0.06668	1.0000	14.9970
0.40679	99.961	0.13267	1.0003	7.5420
0.5	115.439	0.15321	1.0014	6.5453
0.6	130.397	0.17307	1.0041	5.8258
0.7	143.927	0.19102	1.0089	5.3284
0.8	158.266	0.20740	1.0155	4.9727
0.9	167.595	0.22244	1.0243	4.7166
1.0	178.058	0.23632	1.0346	4.5290
1.2	196.824	0.26123	1.0591	4.2940
1.23526	199.896	0.26531	1.0639	4.2667
1.4	213.262	0.28305	1.0870	4.1742
1.6	227.859	0.30242	1.1166	4.1226
1.8	240.966	0.31981	1.1468	4.1122
2.0	252.848	0.33558	1.1769	4.1274
2.5	278.407	0.36951	1.2494	4.2244
3.0	299.593	0.39763	1.3163	4.3575
6.9900	399.722	0.53052	1.6835	5.3423

$$b \frac{dw}{dz} = \frac{j\pi}{2} [m_1 K(m) \operatorname{sn}^2(w/m_1) - E(m)]^{-1}$$

$w = u + jv = \text{complex potential}$

$\operatorname{sn} = \text{Jacobian elliptic function}$

The field deviation Δ from the field at the center of the ground plane is defined as

$$\left| \frac{E_{\text{rel}}(z) - E_{\text{rel}}(0)}{E_{\text{rel}}(0)} \right| = \frac{\left\{ \left[E_{x_{\text{rel}}}(x,y) \right]^2 + \left[E_{y_{\text{rel}}}(x,y) - E_{y_{\text{rel}}}(0,0) \right]^2 \right\}^{\frac{1}{2}}}{\left| E_{y_{\text{rel}}}(0,0) \right|} = \Delta \quad \text{for } b/a \text{ as the parameter} \quad (35)$$

The field deviation contour plots of various values of Δ can be found in figures 4.2 through 4.18 of reference 1, if desired. Presently only maximum deviations are used as shown in table 2.

For a given Δ , we choose the working volume radius a_w where $a_w \approx |z|$ is the maximum radius of a circle inscribed inside the field deviation contour and we constrain $a_w \leq b$. The maximum field deviation for a given ratio a_w/b is given in table 2 with b/a as a parameter; it is plotted as a function of b/a for various a_w/b in figure 5.

The simulator's efficiency ξ is defined by

$$\xi = \frac{V_w}{V_{\text{eq}}} \quad , \quad \frac{\ell}{a_w} \xi = \frac{2\pi a_w^2}{3 \ell c_1 \ell c_3} \quad (36)$$

$$V_w = \frac{2}{3} \pi a_w^3 \quad , \quad a_w = \text{working volume radius}$$

$$V_{\text{eq}} = \text{equivalent volume of the simulator} = \ell \ell c_1 \ell c_3$$

Table 2

MAXIMUM FIELD DEVIATION $10^2 \Delta_{\max}$
 FOR THE FINITE-WIDTH-PLATE SIMULATOR

a_w/b b/a	0.1	0.2	0.3	0.4	0.5	0.6	0.7	0.8	0.9	1.0
0.16670	0.00	0.00	0.00	0.00	0.00	0.00	0.00	0.00	0.00	0.00
0.40679	0.01	0.01	0.02	0.03	0.06	0.08	0.13	0.18	0.26	0.36
0.5	0.01	0.03	0.07	0.13	0.22	0.34	0.51	0.74	1.06	1.49
0.6	0.02	0.09	0.20	0.37	0.61	0.95	1.43	2.06	2.90	4.05
0.7	0.04	0.17	0.40	0.76	1.26	1.96	2.90	4.14	5.75	7.81
0.8	0.08	0.30	0.71	1.31	2.16	3.32	4.84	6.80	9.27	12.28
0.9	0.11	0.46	1.07	1.97	3.22	4.89	7.04	9.73	12.99	16.82
1.0	0.17	0.64	1.47	2.69	4.38	6.57	9.32	12.67	16.59	21.03
1.2	0.25	1.02	2.32	4.19	6.69	9.84	13.62	17.97	22.80	27.94
1.23526	0.27	1.07	2.46	4.45	7.09	10.37	14.30	18.80	23.74	28.95
1.4	0.35	1.38	3.13	5.60	8.80	12.70	17.21	22.21	27.28	32.96
1.6	0.42	1.71	3.85	6.82	10.59	15.04	20.05	25.44	31.00	36.55
1.8	0.50	2.02	4.54	8.08	12.58	17.83	23.42	28.59	33.58	39.15
2.0	0.56	2.28	5.18	9.30	14.64	21.05	28.10	34.87	39.96	41.86
2.5	0.69	2.79	6.42	11.73	18.92	28.07	38.94	50.37	59.72	63.44
3.0	0.78	3.15	7.27	13.45	22.07	33.61	48.22	64.89	79.82	86.14
6.9900	0.96	3.94	9.31	17.78	30.64	50.34	81.58	133.42	216.06	279.12

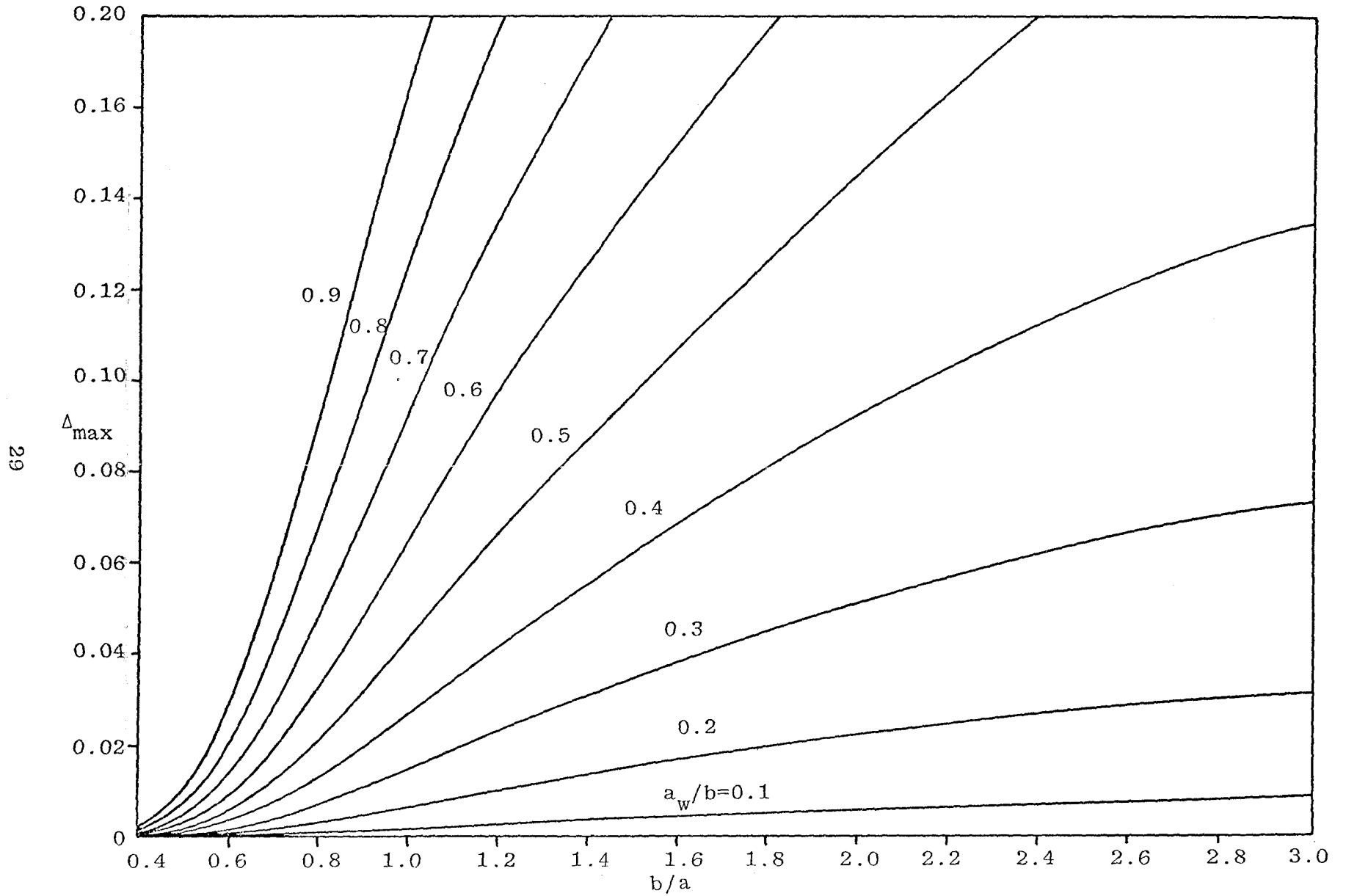


Figure 5. Maximum Field Deviation Δ_{\max} versus b/a for the Finite-Width-Plate Simulator

where l is the length of the simulator. $\xi l/a_w$ versus b/a for field deviation $\Delta = 0.05, 0.1, 0.2, 0.3$ is shown in figure 6. From this we see that $b/a \approx 1.2$ for $\Delta \approx 0.3$ gives the best energy efficiency (Z_c roughly equal to 100 ohms) by the foregoing definitions. Note that the answer is also dependent on Δ .

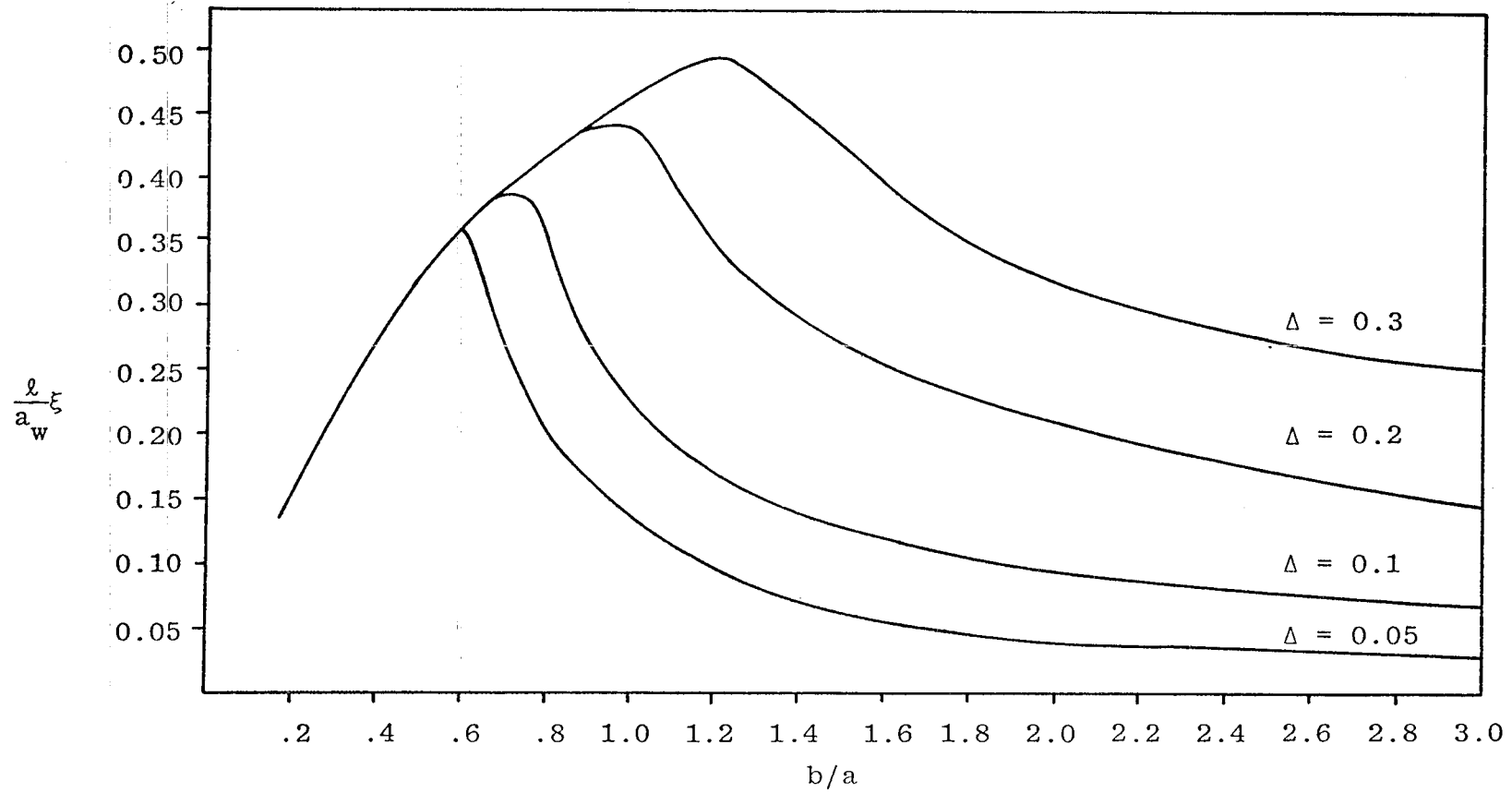


Figure 6. Simulator Efficiency $\xi \ell / a_w$ versus b/a

B. Cylindrical Plate Above Ground Plane

The geometrical impedance factor f_g of a curved plate above ground plane (fig. 7)

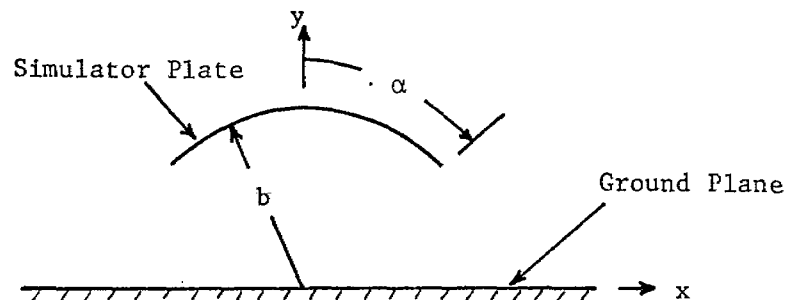


Figure 7. Configuration of Cylindrical Plate Simulator

can be expressed as (ref. 4)

$$2f_g = \frac{K(m)}{K(m_1)}$$
$$\tan(\alpha) = \frac{1 - m^{\frac{1}{2}}}{2m^{\frac{1}{4}}}$$
(37)

The value of f_g is tabulated in table 3 and is also plotted in figure 8. Note that the geometrical impedance factor of a curved plate above the ground plane is equal to one-half of the impedance factor of a cylindrical two-curved-plate transmission line.

4. Tom K. Liu, "Impedances and Field Distribution of Curved Parallel-Plate Transmission-Line Simulators," Sensor and Simulation Note 170, February 1973.

Table 3
 GEOMETRIC IMPEDANCE FACTOR f_g
 FOR THE CYLINDRICAL PLATE SIMULATOR

α (degree)	f_g	α (degree)	f_g	α (degree)	f_g
0	∞	30	0.31982	60	0.19543
1	0.86493	31	0.31433	61	0.19203
2	0.75460	32	0.30900	62	0.18865
3	0.69005	33	0.30381	63	0.18528
4	0.64423	34	0.29875	64	0.18192
5	0.60868	35	0.29383	65	0.17856
6	0.57962	36	0.28902	66	0.17520
7	0.55503	37	0.28432	67	0.17184
8	0.53372	38	0.27972	68	0.16848
9	0.51491	39	0.27523	69	0.16510
10	0.49806	40	0.27082	70	0.16171
11	0.48281	41	0.26651	71	0.15830
12	0.46886	42	0.26227	72	0.15486
13	0.45602	43	0.25811	73	0.15140
14	0.44412	44	0.25402	74	0.14789
15	0.43302	45	0.25000	75	0.14434
16	0.42262	46	0.24605	76	0.14073
17	0.41283	47	0.24215	77	0.13706
18	0.40359	48	0.23831	78	0.13330
19	0.39483	49	0.23452	79	0.12946
20	0.38650	50	0.23078	80	0.12549
21	0.37856	51	0.22709	81	0.12138
22	0.37098	52	0.22344	82	0.11711
23	0.36371	53	0.21983	83	0.11261
24	0.35674	54	0.21626	84	0.10783
25	0.35003	55	0.21272	85	0.10268
26	0.34357	56	0.20921	86	0.09702
27	0.33733	57	0.20573	87	0.09058
28	0.33131	58	0.20227	88	0.08283
29	0.32547	59	0.19884	89	0.07226
30	0.31982	60	0.19543	90	0.

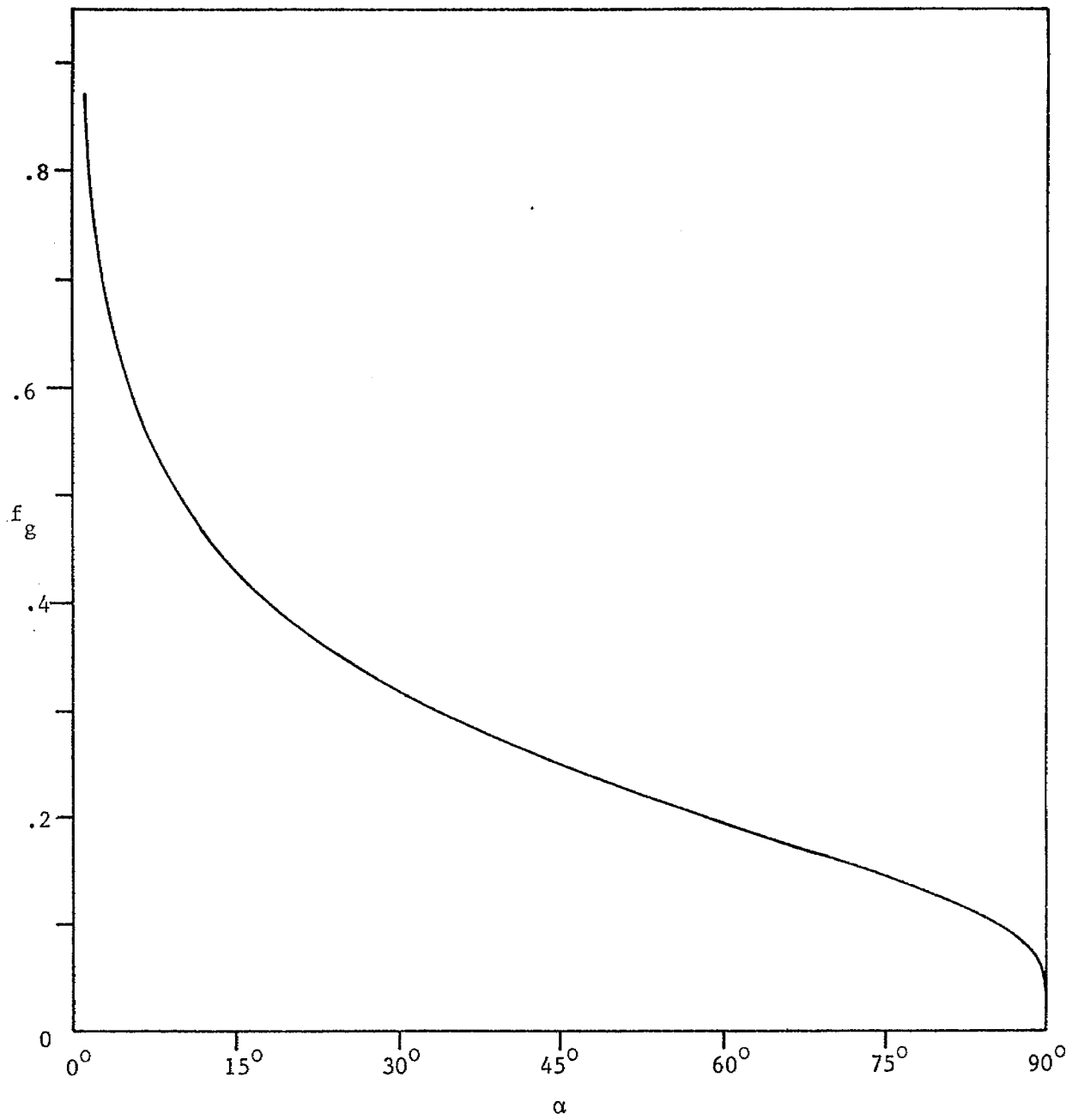


Figure 8. Geometric Factor Versus α for the Cylindrical Plate Simulator

By definition, the conversion length l_{c_1} or l_{c_3} is given by

$$l_{c_3}^{-1} b = \frac{2}{K(m)(1 + m^{\frac{1}{2}})} = f_E = (l_{c_1} f_g)^{-1} b \quad (38)$$

The numerical value of l_{c_3}/b is given in table 4 and f_E and l_{c_3}/b are plotted in figure 9 as a function of α .

To quantify the field uniformity of a simulator, we obtain the complex electric field inside the simulator to be (ref. 4)

$$\frac{E_{rel}(z)}{E_{rel}(0)} = \left\{ \left(\frac{z}{b} \right)^4 + 2 \left[1 - 2 \left(\frac{1 - m^{\frac{1}{2}}}{1 + m^{\frac{1}{2}}} \right)^2 \right] \left(\frac{z}{b} \right)^2 + 1 \right\}^{-\frac{1}{2}} \quad (39)$$

The working volume radius a_w is determined from

$$\left| \frac{E_{rel}(z) - E_{rel}(0)}{E_{rel}(0)} \right| = \Delta \quad (40)$$

Δ is the field deviation and $\Delta \ll 1$ is desirable. Here, we choose $a_w \approx |z|$ to be the radius of a circle inscribed to the field deviation contour for a given Δ .

From the symmetry of the problem, all the odd derivatives of $E_{rel}(z)$ at $z = 0$ vanish. If we let the second derivative of $E_{rel}(z)$ at $z = 0$ be zero, we obtain the maximum field uniformity for $\alpha = 45^\circ$. For $\alpha = 45^\circ$ the maximum allowable working volume radius a_w for a given field deviation Δ is given in table 5 (ref. 4). However, the maximum field deviation Δ_{max} for a given ratio a_w/b is tabulated in table 6 with the simulator's half-span angle α as a parameter. The efficiency ξ of a simulator can be defined by

Table 4

VALUES OF CONVERSION LENGTH l_{c_3}

α (degree)	$l_{c_3} b^{-1}$	α (degree)	$l_{c_3} b^{-1}$	α (degree)	$l_{c_3} b^{-1}$
0	0.	30	1.07826	60	0.84287
1	2.71747	31	1.06496	61	0.83887
2	2.37135	32	1.05233	62	0.83503
3	2.16934	33	1.04018	63	0.83136
4	2.02638	34	1.02853	64	0.82785
5	1.91586	35	1.01736	65	0.82450
6	1.82592	36	1.00663	66	0.82130
7	1.75021	37	0.99633	67	0.81826
8	1.68492	38	0.98644	68	0.81536
9	1.62766	39	0.97693	69	0.81262
10	1.57669	40	0.96779	70	0.81001
11	1.53085	41	0.95900	71	0.80755
12	1.48929	42	0.95054	72	0.80522
13	1.45127	43	0.94240	73	0.80304
14	1.41633	44	0.93457	74	0.80099
15	1.38403	45	0.92703	75	0.79907
16	1.35404	46	0.91979	76	0.79728
17	1.32607	47	0.91280	77	0.79563
18	1.29992	48	0.90608	78	0.79410
19	1.27536	49	0.89961	79	0.79269
20	1.25227	50	0.89338	80	0.79142
21	1.23050	51	0.88739	81	0.79027
22	1.20992	52	0.88162	82	0.78924
23	1.19043	53	0.87609	83	0.78834
24	1.17195	54	0.87075	84	0.78756
25	1.15439	55	0.86562	85	0.78689
26	1.13766	56	0.86070	86	0.78636
27	1.12177	57	0.85596	87	0.78593
28	1.10660	58	0.85142	88	0.78564
29	1.09211	59	0.84706	89	0.78546
30	1.07826	60	0.84287	90	0.78540

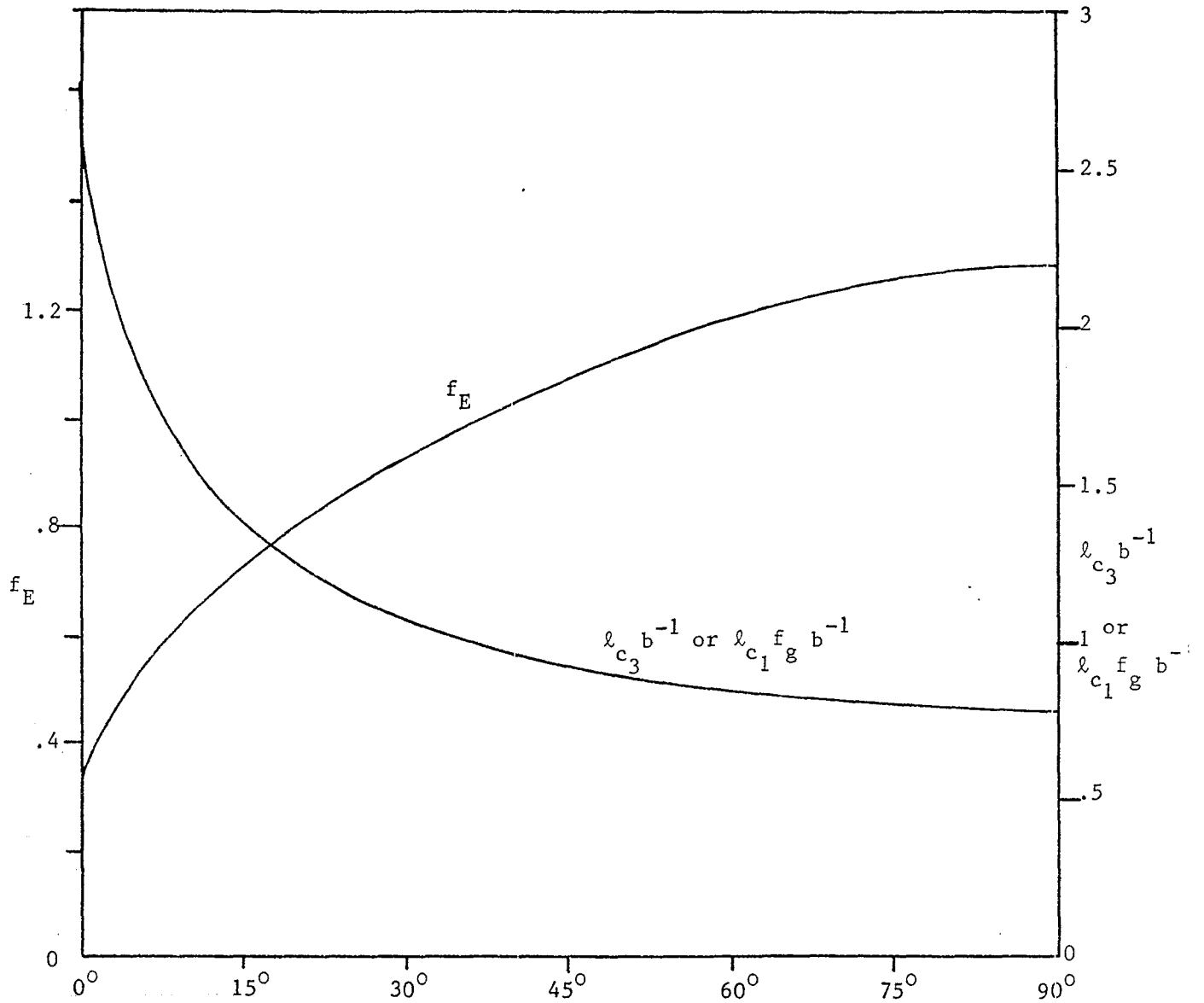


Figure 9. f_E and $\lambda_{c_3} b^{-1}$ or $\lambda_{c_1} f_g b^{-1}$ versus α for a Cylindrical Plate Simulator

Table 5
 PERFORMANCE PARAMETERS
 FOR
 THE CYLINDRICAL PLATE SIMULATOR AT $\alpha = 45^\circ$

Δ	$\frac{a_w}{b}$	$\frac{V_w}{b^3}$	$\frac{V_{eq}}{b^2 l}$	$\frac{\xi l}{a_w}$
0.01	0.35	0.090	3.44	0.075
0.02	0.45	0.191	3.44	0.123
0.05	0.55	0.348	3.44	0.184
0.10	0.65	0.575	3.44	0.257

Table 6
 MAXIMUM FIELD DEVIATION $10^2 \Delta_{\max}$
 FOR THE CYLINDRICAL PLATE SIMULATOR

α (degree) \ / a_w/b	0.1	0.2	0.3	0.4	0.5	0.6	0.7	0.8	0.9
5	0.99	4.10	9.71	18.64	32.44	54.20	90.70	159.02	308.85
10	0.95	3.90	9.18	17.45	29.90	48.57	77.00	119.90	173.39
15	0.87	3.57	8.32	15.59	26.04	40.57	59.84	82.24	98.76
20	0.77	3.12	7.20	13.19	21.31	31.53	42.95	52.66	55.21
25	0.64	2.59	5.86	10.44	16.16	22.46	28.02	33.07	39.11
30	0.50	2.02	4.57	8.16	12.71	18.07	23.97	30.15	36.32
35	0.35	1.42	3.31	6.14	9.96	14.75	20.33	26.43	32.74
40	0.18	0.77	1.91	3.83	6.72	10.72	15.79	21.72	28.16
45	0.00	0.08	0.40	1.25	2.98	5.91	10.20	15.77	22.29
50	0.18	0.77	1.91	3.83	6.72	10.72	15.79	21.72	28.16
55	0.35	1.42	3.31	6.14	9.96	14.75	20.30	26.43	32.74
60	0.50	2.02	4.57	8.16	12.71	18.02	23.97	30.15	36.32
65	0.64	2.59	5.86	10.44	16.16	22.46	28.02	33.07	39.11
70	0.77	3.12	7.20	13.19	21.31	31.53	42.95	52.66	55.21
75	0.87	3.57	8.32	15.59	26.04	40.57	59.84	82.24	98.76
80	0.95	3.90	9.18	17.45	29.90	48.57	77.00	119.90	173.39
85	0.99	4.10	9.71	18.64	32.44	54.20	90.70	159.02	305.85
90	1.01	4.17	9.89	19.05	33.33	56.25	96.08	177.78	526.32

$$\xi = \frac{V_w}{V_{eq}}, \quad \frac{\ell}{a_w} \xi = \frac{2\pi a_w^2}{3\ell c_1 \ell c_3} \quad (41)$$

$$V_{eq} = \text{equivalent volume} = \frac{\ell C'}{\epsilon_0} \ell c_3^2 = \frac{\ell \ell c_3^2}{f_g} = \ell \ell c_1 \ell c_3$$

$$V_w = \text{working volume} = \frac{2}{3} \pi a_w^3$$

where C' denotes the capacitance-per unit length of the simulator and ℓ is the length of the simulator. For $\alpha = 45^\circ$, the efficiency $\xi \ell / b$ is tabulated in table 5.

C. Helmholtz Coils

The Helmholtz coils consist of a pair of N-turn coaxial circular coils separated by a distance equal to their radii ($a =$ radius of each coil = spacing between coils) as shown in figure 10.

The magnetic field inside Helmholtz coils can be expressed in terms of the elliptic integrals and the normalized cylindrical coordinates (R, Z) , where $R = \psi/a$ and $Z = z/a$, by (ref. 5)

$$\vec{H}(R, Z) = H_{\psi}(R, Z) \hat{i}_{\psi} + H_Z(R, Z) \hat{i}_Z \quad (42)$$

Furthermore, the radial and axial field components H_{ψ} and H_Z are given by the sum of the fields due to two coils located at $Z = \pm 0.5$. If each coil is wound with N turns and carries a current I in each turn, we have

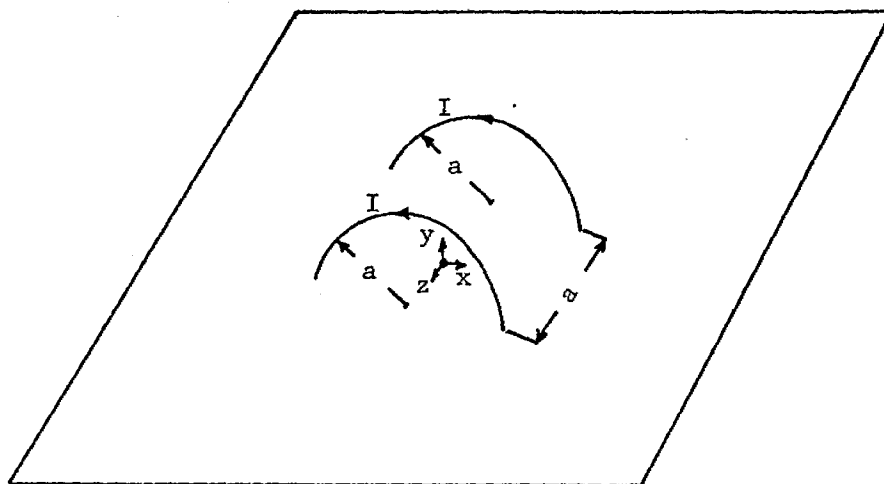
$$\begin{aligned} H_{\psi}(R, Z) &= \frac{NI}{4\pi a} \left[h_{\psi}(R, Z) - h_{\psi}(R, -Z) \right] \\ H_Z(R, Z) &= \frac{NI}{4\pi a} \left[h_Z(R, Z) + h_Z(R, -Z) \right] \end{aligned} \quad (43)$$

$$h_{\psi}(R, Z) = \frac{2(Z-0.5)}{R \left[(1+R)^2 + (Z-0.5)^2 \right]^{\frac{1}{2}}} \left\{ -K(m) + \frac{1 + R^2 + (Z-0.5)^2}{(1-R)^2 + (Z-0.5)^2} E(m) \right\}$$

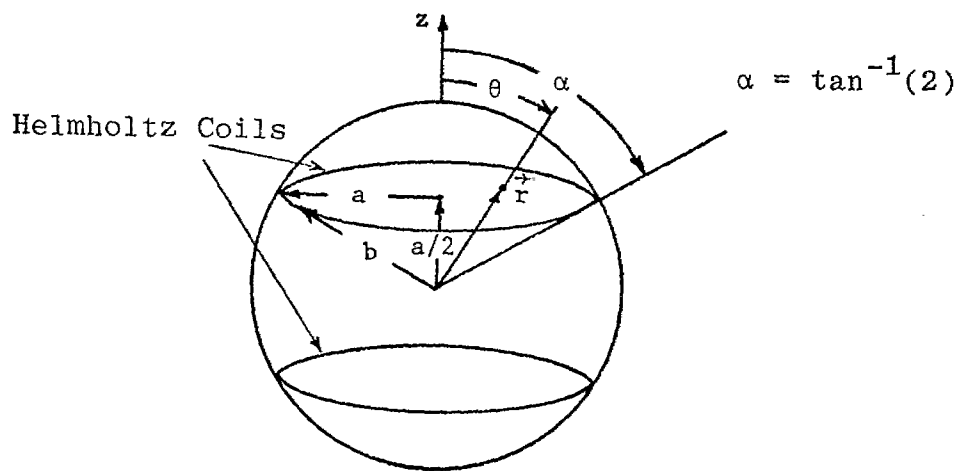
$$h_Z(R, Z) = \frac{2}{\left[(1+R)^2 + (Z-0.5)^2 \right]^{\frac{1}{2}}} \left\{ K(m) + \frac{1 - R^2 - (Z-0.5)^2}{(1-R)^2 + (Z-0.5)^2} E(m) \right\}$$

$$m(Z) = \left[\frac{4R}{(1+R)^2 + (Z-0.5)^2} \right]^{\frac{1}{2}}$$

-
5. K. D. Granzow, "Homogeneity of the Magnetic Field of a Helmholtz Coil," SCR-193, Sandia Corporation Monograph, July 1960.



a. Helmholtz Coil Simulator



b. Helmholtz Coils Arrangement

Figure 10. Geometrical Configuration of Helmholtz Coils

where $K(m)$ and $E(m)$ are the complete elliptic integrals of the first and second kind, respectively. The magnetic field at the center $(R,Z) = (0,0)$ of Helmholtz coils is readily obtained from (43) to be

$$H_z(0,0) = |\vec{H}(0,0)| = \frac{8.992NI}{4\pi a} \quad (44)$$

For the numerical calculations, it is more convenient to express the field as a power series summation in Legendre polynomials. For simplicity, we only consider the z-component magnetic field $H_z(r,\theta)$ in terms of the spherical coordinates (r,θ) in figure 10(b), by using $\vec{H} = \nabla\phi_m$, to give (ref. 6)

$$\begin{aligned} H_z(r,\theta) &= \frac{\sin\theta}{r} \frac{\partial\phi_m}{\partial\theta} - \cos\theta \left(\frac{\partial\phi_m}{\partial r} \right) \\ &= \sum_1^{\infty} n A_n r^{n-1} P_{n-1}(\cos\theta) \end{aligned} \quad (45)$$

ϕ_m = magnetostatic potential

$$= - \sum_1^{\infty} A_n r^n P_n(\cos\theta)$$

Because of the symmetry about the equatorial plane, the terms in odd powers of r are zero and (45) can be rewritten as

$$\begin{aligned} H_z(r,\theta) &= A_1 + \sum_1^{\infty} (2\ell + 1) A_{2\ell+1} r^{2\ell} P_{2\ell}(\cos\theta) \\ &= A_1 (1 + \Delta) \quad \text{for } \ell = 1, 2, 3, \dots \end{aligned} \quad (46)$$

6. J. C. Maxwell, Electricity and Magnetism, Chapter XV, Volume Two, Dover Publications, Inc., New York, 1954.

Δ = field deviation from the field measured at the center of Helmholtz coils

$$= \sum_1^{\infty} (2\ell + 1) \frac{A_{2\ell+1}}{A_1} r^{2\ell} P_{2\ell}(\cos\theta)$$

Note that, in general, the field deviation Δ can be expressed in terms of the magnetic field as

$$\Delta = \left| \frac{\dot{H}(r, \theta) - \dot{H}(0, 0)}{\dot{H}(0, 0)} \right| \quad (47)$$

Assuming that each coil contains N turns and carries a current I , the coefficients A_1 and $A_{2\ell+1}$ are given by

$$A_1 = \frac{8NI}{5\sqrt{5} a} = H_z(0, 0) = \text{field at the center}$$

$$A_{2\ell+1} = \frac{2NI \sin^2(\alpha)}{(2\ell + 1)b^{2\ell+1}} P'_{2\ell+1}(\mu) \quad (48)$$

$$P'_{2\ell+1}(\mu) \equiv \frac{d}{d\mu} P_{2\ell+1}(\mu) \text{ for } \mu = \cos(\alpha)$$

For Helmholtz arrangements b and α are given by (fig. 10)

$$b = \frac{\sqrt{5}}{2} a$$

$$\sin(\alpha) = \frac{2}{\sqrt{5}} \quad (49)$$

$$\cos(\alpha) = \frac{1}{\sqrt{5}}$$

Near the center of Helmholtz coils, the first significant term of Δ is A_5 and thus Δ can be expressed as

$$\Delta = 1.152 \left(\frac{r}{a}\right)^4 P_4(\mu) + \dots \quad (50)$$

$$P_4(\mu) = \frac{1}{8}(35\mu^4 - 30\mu^3 + 3), \quad \mu = \cos(\theta)$$

Since $P_n(\cos\theta) \leq 1$ and $P_n(1) = 1$ for $\theta = 0^\circ$, each term in the power series of Δ is greatest on the axis. Define a working volume radius a_w to quantify the field uniformity of Helmholtz coils. For a given working volume radius a_w , we have the maximum field deviation Δ_{\max} to be (near the center of Helmholtz coils)

$$\Delta_{\max} = \left| \frac{\{[H_Z(r,\theta) - H_Z(0,0)]^2 + H_\Psi^2(r,\theta)\}^{\frac{1}{2}}}{H_Z(0,0)} \right|_{\text{on the axis}} \quad (51)$$

The numerical values of Δ_{\max} can be found in table 7 (ref. 7) with working-volume-to-loop radii ratio as a parameter.

The conversion length of the Helmholtz coils type of the H-field simulator can be obtained readily from (48) to be

$$l_{c_m} = \frac{\text{input current } I}{\text{magnetic field at the center } H_Z(0,0)} = \frac{5\sqrt{5} a}{8N} \quad (52)$$

Subscript m, $m = 1$ or 2 , indicates the conversion length having two degrees of freedom corresponding to the orientations of Helmholtz coil, i.e., the axis of the coils can be along two orthogonal vectors tangential to the ground plane.

The inductance of Helmholtz coils can be expressed as the sum of the self-inductance L_{self} and mutual inductance M of the constituent-current loops to give

7. J. E. Everett and J. E. Osemeikhian, "Spherical Coils for Uniform Magnetic Fields," J. Sci. Instrum, Vol. 43, pp. 470-474, 1966.

Table 7
 MAXIMUM FIELD DEVIATION
 OF
 THE HELMHOLTZ-COILS SIMULATOR

a_w/a	$10^6 \Delta_{\max}$	a_w/a	$10^3 \Delta_{\max}$
0	0		
0.01	0.01	0.10	0.11
0.02	0.18	0.15	0.57
0.03	0.83	0.20	1.8
0.04	2.9	0.25	4.2
0.06	15	0.30	8.4
0.08	47	0.40	25
		0.50	54

$$L = L_{\text{self}} + M$$

Here, the self and mutual inductances of the (half) circular loops can be found in reference 8 to be

$$L_{\text{self}} \approx \mu a N^2 \left[\ln \left(\frac{8a}{r_w} \right) - 2 \right] \quad (53)$$

$$M = \frac{\mu a N^2}{2} \left[\frac{3}{\sqrt{5}} K(m) - \sqrt{5} E(m) \right] = 0.47251 \mu a N^2, \\ m = \frac{2}{\sqrt{5}}$$

where r_w is approximately the radius of the bundle of N wires (assumed closely packed) in each coil and $K(m)$ and $E(m)$ are complete elliptic integrals of the first and second kinds, respectively.

The efficiency of the Helmholtz-coils simulator can be written as

$$\xi_h = \frac{\mu}{L} \frac{V_w}{\ell_{c_m}^2}, \quad V_m = \frac{2\pi a_w^2}{3}$$

or

$$\frac{L}{4N^2 \mu a} \xi_h = 0.268 \left(\frac{a_w}{a} \right)^3 \quad (54)$$

The coil inductance L and the simulator's conversion length ℓ_{c_m} are obtained from (53) and (52). Some numerical values of $\xi_h L / (4N^2 \mu a)$ are tabulated in table 8. The normalization constant $L / (4N^2 \mu a)$ is a function of a/r_w and can be evaluated by

$$L / (4N^2 \mu a) = 0.25 \ln(8a/r_w) - 0.38187 \approx 1.46 \text{ for } a/r_w = 200$$

8. W. R. Smythe, Static and Dynamic Electricity, Chapter VIII, 3rd ed., McGraw-Hill Book Co., New York, 1968.

Table 8
 VALUES OF SIMULATOR'S EFFICIENCY ξ_h
 FOR HELMHOLTZ COILS

$\frac{a_w}{a}$	$\frac{10^2 L}{4N^2 \mu a} \xi_h$	Δ_{\max}
0.15	0.09	0.00057
0.20	0.21	0.0018
0.25	0.42	0.0042
0.30	0.72	0.0084
0.40	1.72	0.025
0.50	3.35	0.054

D. Maxwell Coils

Maxwell coils consist of three circular coils wound on a spherical surface of radius b as shown in figure 11. If the coils are connected in series and carry current I in each turn, a typical number N_1 of windings in the center coil (large coil) is 64 and the number N_2 of windings in each of the other two coils is 49. The radius of each of the smaller coils is $\sqrt{4/7} b$ and the distance of either of them from the plane of the center coil is $\sqrt{3/6} b$ (ref. 6).

The magnetostatic potential ϕ_m of Maxwell coils is given by, similar to (45),

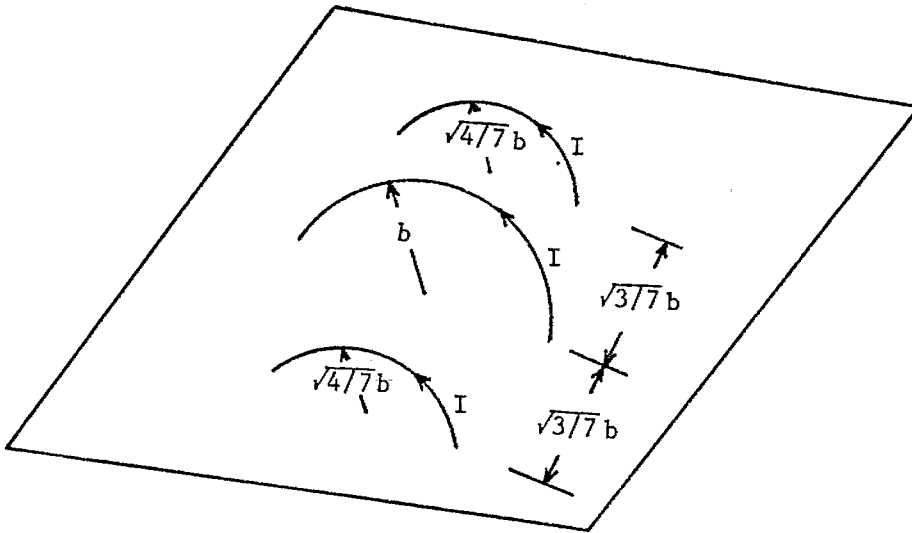
$$\phi_m = - \sum_1^{\infty} A_n r^n P_n(\cos\theta) \quad (55)$$

The magnetic field component in the z-axis is obtained from (55) to be

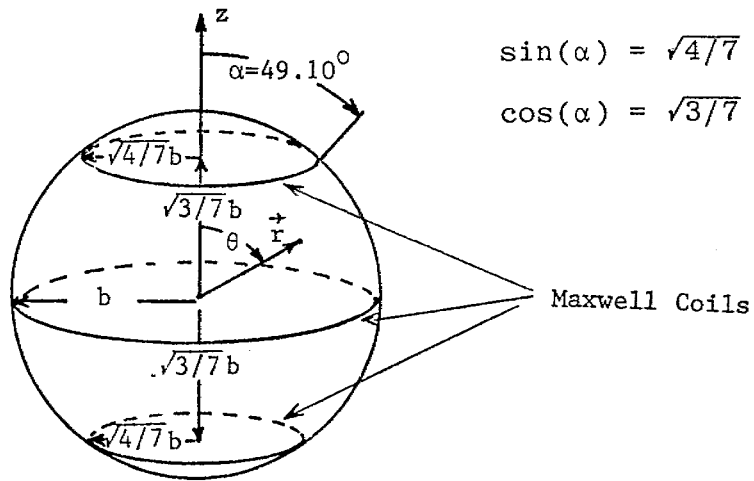
$$\begin{aligned} H_z(r, \theta) &= \frac{\sin\theta}{r} \frac{\partial \phi_m}{\partial \theta} - \cos\theta \frac{\partial \phi_m}{\partial r} \\ &= \sum_1^{\infty} n A_n r^{n-1} P_{n-1}(\cos\theta) \end{aligned} \quad (56)$$

Again, because of the symmetry of the problem, the terms in the odd power of r vanish and (56) is reduced to

$$\begin{aligned} H_z(r, \theta) &= A_1 + \sum_1^{\infty} (2\ell + 1) A_{2\ell+1} r^{2\ell} P_{2\ell}(\cos\theta) \\ &= A_1(1 + \Delta) \quad \text{for } \ell = 1, 2, 3, \dots \end{aligned} \quad (57)$$



a. Maxwell Coils Simulator



b. Maxwell Coils Arrangement

Figure 11. Geometrical Configuration of Maxwell Coils

where Δ is the field deviation given by

$$\Delta = \sum_1^{\infty} (2\ell + 1) \frac{A_{2\ell+1}}{A_1} r^{2\ell} P_{2\ell}(\cos\theta) \quad (58)$$

The coefficients A_1 and $A_{2\ell+1}$ are found to be

$$A_1 = \frac{N_1 I}{b} + \frac{2N_2 I \sin^2(\alpha)}{b}$$

$$A_{2\ell+1} = N_1 I (-1)^\ell \frac{1 \cdot 3 \cdots (2\ell - 1)}{2 \cdot 4 \cdots 2\ell} P'_{2\ell+1}(\mu) \quad (59)$$

$$P'_{2\ell+1}(\mu) = \frac{d}{d\mu} P_{2\ell+1}(\mu), \quad \mu = \cos(\alpha)$$

Let the Maxwell coils arrangement be

$$N_1 = 64, N_2 = 49, \sin(\alpha) = \sqrt{4/7} \text{ and } \cos(\alpha) = \sqrt{3/7} \quad (60)$$

the first several significant terms in (57) are

$$A_1 = \frac{120I}{b} = H_z(0,0)$$

$$A_3 = A_5 = 0$$

$$A_7 = -\frac{2.043}{7b^6} A_1$$

$$A_9 = \frac{2.878}{9b^8} A_1$$

(61)

Therefore, the field deviation can be expressed as a sum of power series:

$$\Delta = -2.043\left(\frac{r}{b}\right)^6 P_6(\cos\theta) + 2.878\left(\frac{r}{b}\right)^8 P_8(\cos\theta) - \cdots \quad (62)$$

$$P_6(\mu) = \frac{1}{16}(231\mu^6 - 315\mu^4 + 105\mu^2 - 5) , \quad \mu = \cos(\theta)$$

$$P_8(\mu) = \frac{1}{128}(6435\mu^8 - 12012\mu^6 + 6930\mu^4 - 1260\mu^2 + 35)$$

By using the same argument given in the previous subsection, the maximum field deviation Δ_{\max} is calculated on the axis for a given working volume radius a_w to be (near the center of coils)

$$\begin{aligned} \Delta_{\max} &= \left| \frac{H_z(r, \theta) - H_z(0, 0)}{H_z(0, 0)} \right|_{\text{on the axis}} & (63) \\ &= 2.043\left(\frac{z}{b}\right)^6 - 2.878\left(\frac{z}{b}\right)^8 + \dots \end{aligned}$$

The numerical values of Δ_{\max} are given in table 9 for varying a_w/b .

The conversion length of the Maxwell coils simulator can be obtained from (59) to be

$$\begin{aligned} l_{c_m} &= \frac{I}{H_z(0, 0)} \\ &= \frac{b}{N_1 + 2N_2 \sin^2(\alpha)} = \frac{1.35}{N_1 + 2N_2} b, \quad m = 1 \text{ or } 2 & (64) \end{aligned}$$

The inductance of Maxwell coils is given by the summation of the self and mutual inductance of the coils:

$$L = L_{\text{self}} + M$$

$$\begin{aligned} L_{\text{self}} &= \text{self-inductance of the coils} \\ &= L_1 + 2L_2 \end{aligned}$$

Table 9
 MAXIMUM FIELD DEVIATION
 OF
 THE MAXWELL-COILS SIMULATOR

a_w/b	$10^9 \Delta_{\max}$	a_w/b	$10^5 \Delta_{\max}$
0	0	0.10	0.20
0.01	0.002	0.15	2.25
0.02	0.13	0.20	12.34
0.03	1.49	0.25	45.49
0.04	8.35	0.30	130
0.06	94.83	0.40	648
0.08	530.73	0.50	2068

$$\begin{aligned}
M &= \text{mutual inductance of the coils} \\
&= 2M_{12} + M_{22}
\end{aligned}$$

From reference 8, the self and mutual inductances of the (half) circular loops are given by, for $N_1 = 64$ and $N_2 = 49$,

$$\begin{aligned}
L_1 &\approx \frac{\mu b N_1^2}{2} \left[\ln \left(\frac{8b}{r_{w1}} \right) - 2 \right] = 2048 \mu b \left[\ln \left(\frac{8b}{r_{w1}} \right) - 2 \right] \\
L_2 &\approx \mu b N_2^2 \sin(\alpha) \left[\ln \left(\frac{8b \sin(\alpha)}{r_{w2}} \right) - 2 \right] = 2401 \mu b \left[\ln \left(\frac{8b}{r_{w2}} \right) - 2.28 \right] \\
M_{12} &= \mu b \left[\frac{1 + \sin(\alpha)}{2} \right]^{\frac{1}{2}} N_1 N_2 \left[\frac{1}{1 + \sin(\alpha)} K(m) - E(m) \right] = 1398.37 \mu b, \\
&\hspace{25em} m = \kappa_{12} \\
M_{22} &= \mu b N_2^2 \left[\frac{1 + \cos^2(\alpha)}{2} K(m) - E(m) \right] = 818.35 \mu b, \quad m = \kappa_{22} \\
\kappa_{12} &= \left(\frac{2 \sin(\alpha)}{1 + \sin(\alpha)} \right)^{\frac{1}{2}} = \left(\frac{2\sqrt{4/7}}{1 + \sqrt{4/7}} \right)^{\frac{1}{2}} = 0.92790 \\
\kappa_{22} &= \sin(\alpha) = \sqrt{4/7} = 0.75593
\end{aligned} \tag{65}$$

r_{w1}, r_{w2} = radius of bundles of N_1 wires and N_2 wires (assumed closely packed) in each coil

The efficiency of the Maxwell-coils simulator is defined by

$$\begin{aligned}
\xi_h &= \frac{\mu}{L} \frac{V_w}{l_{cm}^2} \\
\frac{L}{(N_1 + 2N_2)^2 \mu b} \xi_h &= 1.149 \left(\frac{a_w}{b} \right)^3
\end{aligned} \tag{66}$$

The numerical values of $\xi_h L / [(N_1 + 2N_2)^2 \mu b]$ are given in table 10 and the normalization constant $L / [(N_1 + 2N_2)^2 \mu b]$ can be expressed as,

Table 10

VALUES OF SIMULATOR'S EFFICIENCY ξ_h
FOR MAXWELL COILS

$\frac{a_w}{b}$	$\frac{10^2 L}{(N_1+2N_2)^2 \mu b} \xi_h$	$10^5 \Delta_{max}$
0.10	0.11	0.20
0.15	0.39	2.25
0.20	0.92	12.34
0.25	1.80	45.49
0.30	3.10	130
0.40	7.35	648
0.50	14.36	2068

for $N_1 = 64$ and $N_2 = 49$

$$\frac{L}{[(N_1 + 2N_2)^2 \mu b]} = 0.07804 \left[\ln \left(\frac{8b}{r_{w1}} \right) - 2 \right] \\ + 0.18298 \left[\ln \left(\frac{8b}{r_{w2}} \right) - 2.28 \right] + 0.13775$$

If $r_{w1} = r_{w2} = r_w$ and $b/r_w = 200$, we obtain

$$\frac{L}{[(N_1 + 2N_2)^2 \mu b]} = 0.26102 \ln \left(\frac{8b}{r_w} \right) - 0.43552 \approx 1.49$$

Comparing tables 8 and 10, we see that the Maxwell-coils simulator produces much more uniform field near the center than the Helmholtz-coils simulator. Also, if we assume the normalization constants $L/[(2N)^2 \mu a] \approx 1.46$ for $a/r_w = 200$ and $L/[(N_1 + 2N_2)^2 \mu b] \approx 1.49$ for $b/r_w = 200$ to be approximately equal, then the Maxwell-coils simulator has four times better efficiency than the Helmholtz-coils simulator.

IV. Simulator/Object Interaction Canonical Problems

A. Half Cylinder Between Infinite Large Plate and Ground Plane

The change of the admittance of a large plate simulator above the ground plane due to the presence of a cylindrical test object of radius d , as shown in figure 12, inside the simulator is given by

$$\frac{\Delta Y_L}{Y_O} = \frac{\pi}{2} \left(\frac{d}{2b}\right)^2 C_1 \quad (67)$$

Y_O = characteristic admittance of medium (or free space)

The Fourier coefficients C_{2n-1} ($C_1 \equiv C_{2n-1}$ for $n = 1$) for the calculation of the surface charge density induced on the cylinder can be expressed as ($n > 0$)

$$C_{2n-1} = \delta_{n,1} + 2 \sum_{m=1}^{\infty} \left(\frac{d}{2b}\right)^{2(m+n-1)} \begin{bmatrix} 2m+2n-1 \\ 2n-2 \end{bmatrix} \zeta(2n+2m) C_{2m-1} \quad (68)$$

where $\zeta(z)$ is the Riemann zeta function and the numerical values of C_{2n-1} are given by table 11 (ref. 9).

The increment of the simulator's admittance due to the presence of the half-cylinder inside the simulator is plotted in figure 13 (ref. 8).

-
9. R. W. Latham, "Interaction Between a Cylindrical Test Body and a Parallel Plate Simulator," Sensor and Simulation Note 55, May 1968.

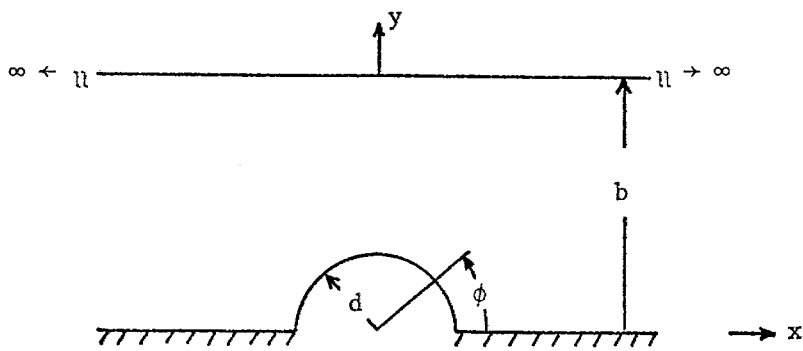


Figure 12. A Half Cylinder Inside an Infinite Large Plate Simulator and the Ground Plane

Table 11

FOURIER COEFFICIENTS FOR CALCULATION
 OF THE CYLINDER SURFACE CHARGE DENSITY $\sigma(\phi)$
 WHERE $\sigma(\phi) = -2\epsilon E_0(C_1 \sin\phi + C_3 \sin 3\phi + C_5 \sin 5\phi + \dots)$

Coeff. d/b	C ₁	C ₃	C ₅	C ₇	C ₉	C ₁₁
0.00	1.000					
0.04	1.001					
0.08	1.005					
0.12	1.012					
0.16	1.022					
0.20	1.034	0.001				
0.24	1.050	0.001				
0.28	1.069	0.003				
0.32	1.092	0.005				
0.36	1.119	0.008				
0.40	1.152	0.012	0.001			
0.44	1.190	0.018	0.001			
0.48	1.234	0.027	0.002			
0.52	1.287	0.038	0.004			
0.56	1.349	0.054	0.007	0.001		
0.60	1.423	0.076	0.011	0.001		
0.64	1.512	0.105	0.017	0.003		
0.68	1.621	0.145	0.027	0.005	0.001	
0.72	1.756	0.201	0.043	0.008	0.001	
0.76	1.930	0.280	0.069	0.015	0.003	0.001
0.80	2.160	0.395	0.112	0.029	0.007	0.001

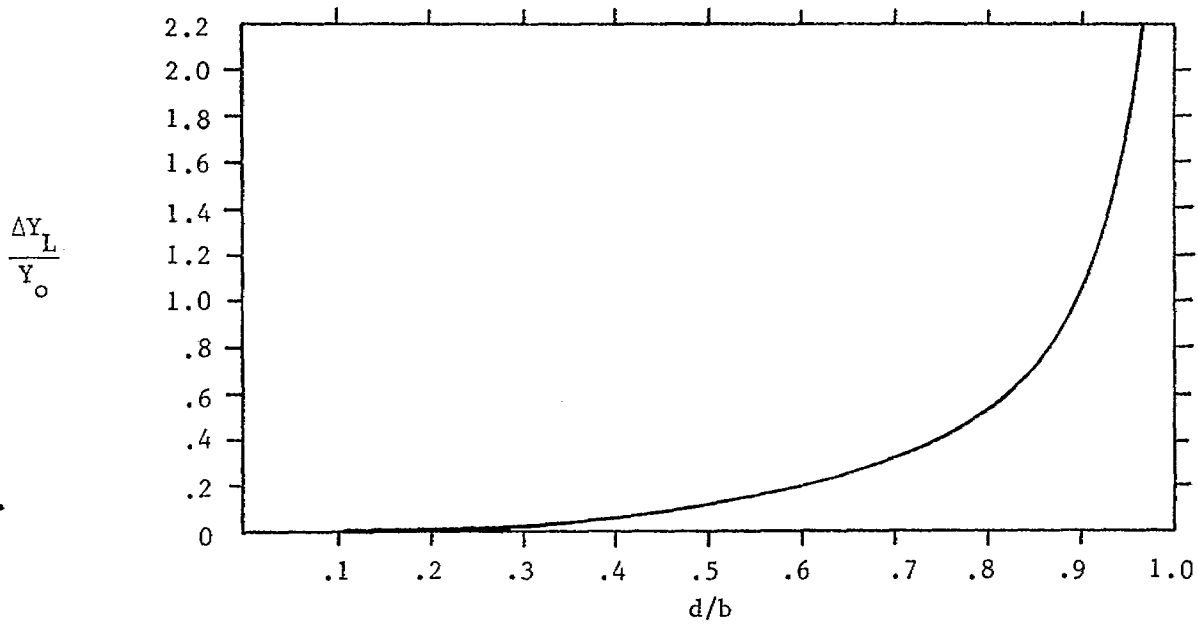


Figure 13. Increment Admittance Due to the Half-Cylinder Inside the Large Plate Simulator

The change of the surface charge density on the cylinder with respect to the charge density induced on the same cylinder immersed in a uniform electric field E_0 can be expressed by

$$\Delta_{SO}(\phi) = \left| \frac{\sigma(\phi) - \sigma_{\infty}(\phi)}{\sigma_{\infty}(\phi)} \right|$$

$$\sigma(\phi) = -2\epsilon E_0 \sum_{n=1}^{\infty} C_{2n-1} \sin[(2n-1)\phi] \quad (69)$$

$$\sigma_{\infty}(\phi) = \sigma(\phi) \Big|_{\substack{b \rightarrow \infty \\ E_0 = \text{constant}}} = \text{charge induced on the cylinder when the cylinder is immersed in a uniform electric field } E_0$$

$$= -2\epsilon E_0 \sin \phi$$

$$E_0 = \frac{V_0}{b} = \text{electric field at the center of the ground plane with the test object removed (i.e., a smooth conducting ground plane)}$$

The increment of the charge density $\Delta_{SO}(\phi)$ for $\phi = 30^\circ, 60^\circ, 90^\circ$ are given by table 12 with d/b as the parameter. However, the maximum increment of the charge density is evaluated at $\phi = 90^\circ$.

B. Half Cylinder Between a Finite-Width Plate and Ground Plane

The change of the geometrical impedance factor of the finite-width-plate simulator above ground plane (figure 14) due to the presence of the cylinder can be given by

$$\frac{\Delta f_g}{f_{g_0}} = \frac{f_g}{f_{g_0}} - 1 \quad (70)$$

Here, f_{g_0} denotes the geometrical impedance factor of the simulator without the presence of the circular cylinder.

Table 12

INCREMENT OF SURFACE CHARGE DENSITY $\Delta_{SO}(\phi)$, $\phi = 30^\circ, 60^\circ, 90^\circ$
ON A HALF CYLINDER INSIDE LARGE PLATE SIMULATOR

$d/b \backslash \phi$	30°	60°	90°
0.04	0.002	0.001	0.001
0.08	0.006	0.006	0.005
0.12	0.012	0.012	0.012
0.16	0.020	0.022	0.022
0.20	0.032	0.033	0.035
0.24	0.046	0.050	0.051
0.28	0.064	0.069	0.072
0.32	0.082	0.092	0.097
0.36	0.104	0.119	0.127
0.40	0.128	0.151	0.164
0.44	0.154	0.188	0.209
0.48	0.184	0.231	0.263
0.52	0.214	0.282	0.329
0.56	0.248	0.341	0.411
0.60	0.282	0.410	0.511
0.64	0.320	0.492	0.637
0.68	0.360	0.589	0.799
0.72	0.404	0.706	1.011
0.76	0.448	0.846	1.298
0.80	0.498	1.022	1.705

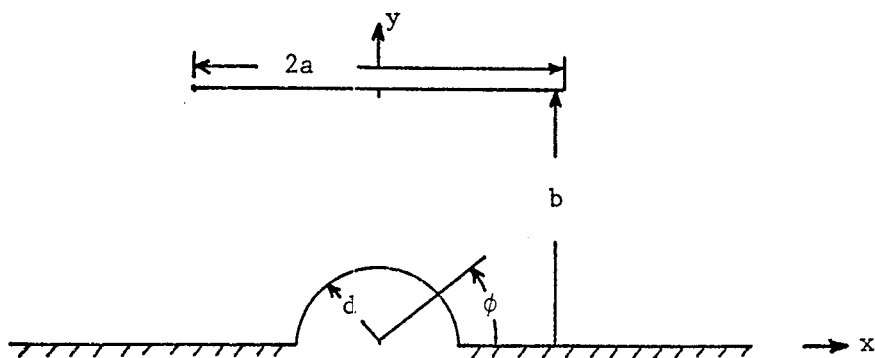


Figure 14. A Half-Cylinder Inside a Finite-Width-Plate Simulator and the Ground Plane

The numerical values of $\Delta f_g/f_{g_0}$ are tabulated in table 13 and are also shown in figure 15 (ref. 10). From table 13, it shows that for a given d/b , $\Delta f_g/f_{g_0}$ is not sensitive to the variation of the simulator width-to-height ratio, a/b . For a/b greater than one, values of $\Delta f_g/f_{g_0}$ can be thought of in the context of the infinite plate case.

The change of the surface charge density on the cylinder compared to the induced surface charge density on the same cylinder immersed in a uniform electric field E_0 can be given by

$$\Delta_{SO}(\phi) = \left| \frac{\sigma(\phi) - \sigma_{\infty}(\phi)}{\sigma_{\infty}(\phi)} \right|$$

$$\sigma(\phi) = 2\pi\epsilon E_0 (b/a) \sum_{k=1}^{\infty} A_{2k-1} \sin[(2k-1)\phi] \quad (71)$$

$$\sigma_{\infty}(\phi) = \sigma(\phi) \Big|_{\substack{b \rightarrow \infty \\ E_0 = \text{constant}}} = -2\pi\epsilon E_0 \frac{\sin \phi}{2K(m_1) E(m)}$$

where E_0 is the electric field at the center of the ground plane without the presence of the cylinder.

The Fourier coefficients A_{2k-1} ($k > 0$) are given by table 14 and the increment of the charge density $\Delta_{SO}(\phi)$ along the surface of the cylinder is given by table 15 (ref. 9).

10. Soon K. Cho and Chiao-Min Chu, "A Parametric Study of a Circular Cylinder within Two Parallel Plates of Finite Width," Sensor and Simulation Note 174, January 1973.

Table 13

INCREMENT OF GEOMETRICAL IMPEDANCE $\Delta f_g / f_{g_0}$
 OF A FINITE-WIDTH SIMULATOR DUE TO THE HALF CYLINDER
 INSIDE THE SIMULATOR WITH d/b and a/b AS PARAMETERS

$d/b \backslash a/b$	0.1	0.2	0.5	1.0
0.1	-0.00537	-0.00641	-0.00761	-0.00694
0.2	-0.02147	-0.02565	-0.03047	-0.02899
0.3	-0.04841	-0.05781	-0.06867	-0.06311
0.4	-0.08654	-0.10329	-0.02250	-0.11323
0.5	-0.13688	-0.16308	-0.19258	-0.17915
0.6	-0.20169	-0.23947	-0.28022	-0.26437
0.7	-0.28601	-0.33722	-0.38799	-0.36495
0.8	-0.40151	-0.46635	-0.52101	-0.49195
0.9	-0.58110	-0.65042	-0.69112	-0.65589
0.99	-0.92472	-0.92978	-0.92334	-0.90017

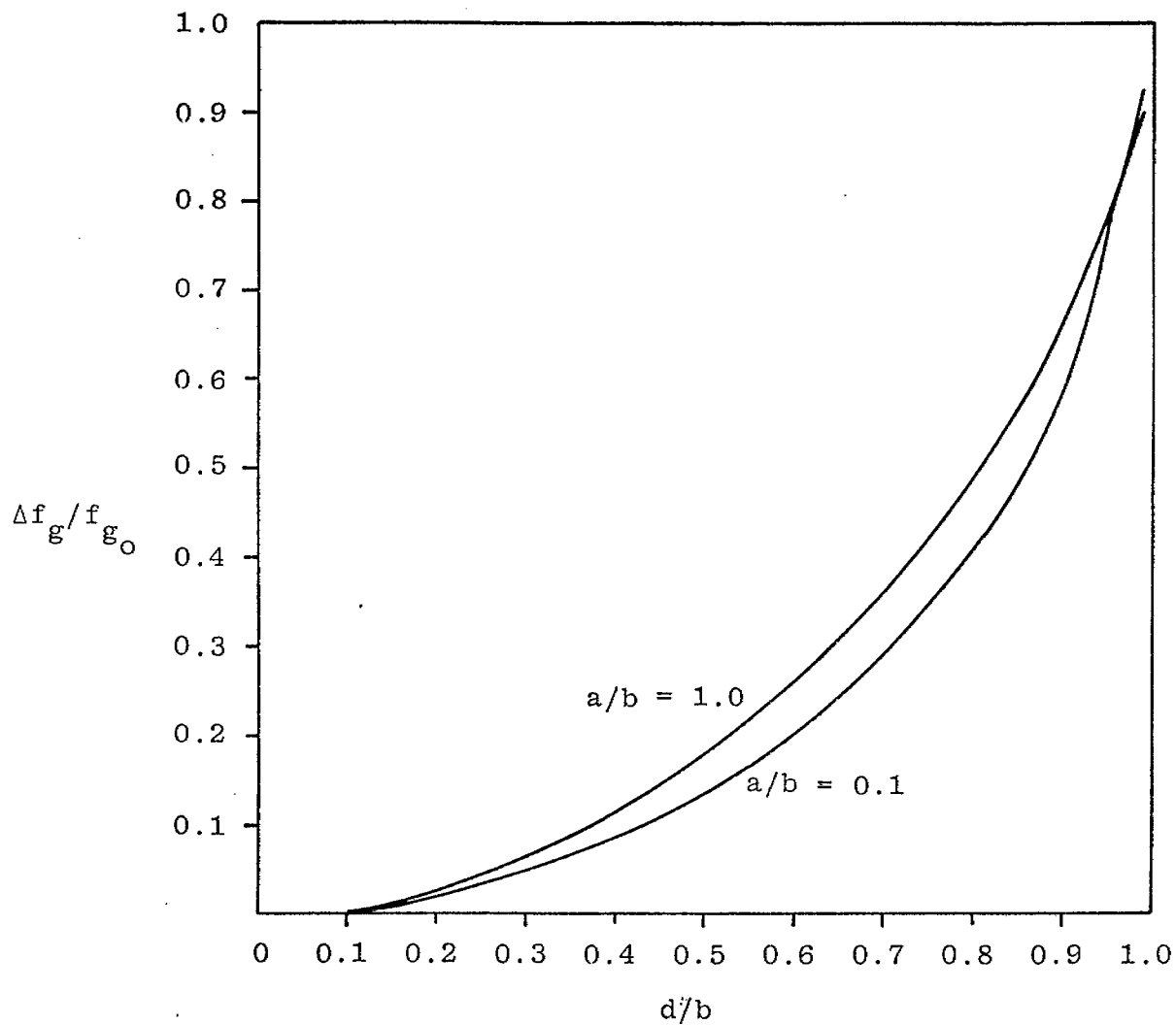


Figure 15. Increment of Geometrical Impedance Factor $\Delta f_g / f_{g_0}$ versus d/b

Table 14

FOURIER COEFFICIENTS A_n FOR CALCULATION
 OF THE SURFACE CHARGE DENSITY $\sigma(\phi)$ ON THE CYLINDER
 WHERE $\frac{a/b}{2\pi\epsilon E_0} \sigma(\phi) = (A_1 \sin\phi + A_3 \sin 3\phi + A_5 \sin 5\phi + \dots)$

	A_n d/b	A_1	A_3	A_5	A_7	A_9	A_{11}
a/b = 0.1	0	-0.0172					
	0.1	-0.0172					
a/b = 0.2	0	-0.0418					
	0.1	-0.0418					
	0.2	-0.0427					
a/b = 0.5	0	-0.1352					
	0.2	-0.140					
	0.5	-0.168	0.006				
	0.99	-0.452	0.077	-0.01			
a/b = 1.0	0	-0.3077					
	0.1	-0.31					
	0.2	-0.318					
	0.4	-0.354	0.0018				
	0.6	-0.438	0.015				
	0.8	-0.667	0.1	-0.01	0.022		
	0.9	-1.03	0.32	-0.085	0.029	-0.011	0.003
a/b = 2.0	0	-0.637					
	0.08	-0.640					
	0.16	-0.651					
	0.24	-0.668					
	0.32	-0.695	0.003				
	0.40	-0.733	0.008				
	0.48	-0.786	0.017				
	0.56	-0.859	0.034	-0.004	0.001		
	0.64	-0.963	0.067	-0.011	0.002		
	0.72	-1.118	0.128	-0.027	0.005	-0.002	0.001
	0.80	-1.375	0.251	-0.071	0.008	-0.007	0.001

Table 15

INCREMENT OF SURFACE CHARGE DENSITY $\Delta_{SO}(\phi)$ for $\phi = 30^\circ, 60^\circ, 90^\circ$
DUE TO A HALF CYLINDER INSIDE THE FINITE-WIDTH-PLATE SIMULATOR

	$d/b \backslash \phi$	30°	60°	90°
a/b = 0.1	0.1	0.0	0.0	0.0
	0.2	0.0215	0.0215	0.0215
a/b = 0.2	0.1	0.0	0.0	0.0
	0.2	0.0215	0.0215	0.0215
	0.5	0.154	0.243	0.287
a/b = 0.5	0.2	0.0355	0.0355	0.0355
	0.5	0.154	0.243	0.287
	0.99	1.278	2.269	2.987
a/b = 1.0	0.1	0.0075	0.0075	0.0075
	0.2	0.0335	0.0335	0.0335
	0.4	0.139	0.151	0.156
	0.6	0.326	0.423	0.472
	0.8	0.622	1.063	1.597
	0.9	0.577	1.987	3.803
a/b = 2.0	0.08	0.005	0.005	0.005
	0.16	0.022	0.022	0.022
	0.24	0.049	0.049	0.049
	0.32	0.083	0.091	0.096
	0.40	0.127	0.151	0.163
	0.48	0.181	0.234	0.261
	0.56	0.250	0.341	0.410
	0.64	0.322	0.492	0.637
	0.72	0.404	0.706	1.006
	0.80	0.498	1.022	1.705

For a/b greater than one, A_{2k-1} can be approximated by using the simple relation

$$|A_{2k-1}| = \frac{a/b}{\pi} C_{2k-1} \quad (72)$$

Here, C_{2k-1} is Fourier coefficients of infinite plate case and is tabulated in table 11. If (72) is used to calculate A_{2k-1} for $a/b = 1$, the error of the leading term coefficient A_1 of charge density $\sigma(\phi)$ is found to be less than 0.04. In table 15 the increment of charge density Δ_{SO} for $a/b = 2.0$ is calculated by using (72).

C. Prolate Hemispheroid Inside a Half Circular Loop

The test object inside a current loop simulator is a perfectly conducting prolate hemispheroid of major and minor axes $2d$ and $2b$ ($d \geq b$), respectively, situated on a perfectly conducting ground plane (fig. 16). The spheroidal coordinates ξ, η, ϕ of figure 17 are used to define the circular loop by $\eta = \eta_0$ and $\xi = 0$ and the test body by $\eta = \eta_1$ (ref. 11).

The change of the magnetic field (equivalent to the skin current on the spheroid) on the surface of the spheroid compared to the induced magnetic field on the surface of the same test body immersed in a uniform magnetic field H_0 can be given by

$$\Delta_{so} = \left| \frac{H(\xi, \eta_1) - H_\infty(\xi, \eta_1)}{H_\infty(\xi, \eta_1)} \right| \text{ on the surface of the spheroid}$$

$$H(\xi, \eta_1) = \frac{H_0}{\sqrt{(d/b)^2 - 1}} \frac{\eta_0^2 - 1}{(\eta_1^2 - 1)\sqrt{\eta_1^2 - \xi^2}} \sum_{n=\text{odd}}^{\infty} \frac{2n+1}{n(n+1)} P_n^1(0) P_n^1(\xi) \frac{Q_n^1(\eta_0)}{Q_n^1(\eta_1)}$$

$$H_\infty(\xi, \eta_1) = H(\xi, \eta_1) \Big|_{\substack{\eta_0 \rightarrow \infty \\ H_0 = \text{constant}}} = \text{induced field on spheroid when the spheroid is immersed in a homogeneous magnetic field } H_0$$

$$= \frac{-H_0}{(\eta_1^2 - \xi^2)(\eta_1^2 - 1)} \frac{P_1^1(\xi)}{Q_1^1(\eta_1)} \quad (73)$$

$$H_0 = \frac{I}{2a} = \text{field at the center of the current loop without the presence of the spheroid (a smooth conducting plane)}$$

11. A. D. Varvatsis and M. I. Sancer, "Low-Frequency Magnetic Field Interaction of a Half Toroid Simulator with a Perfectly Conducting Half Prolate Spheroid," Sensor and Simulation Note 131, June 1971.

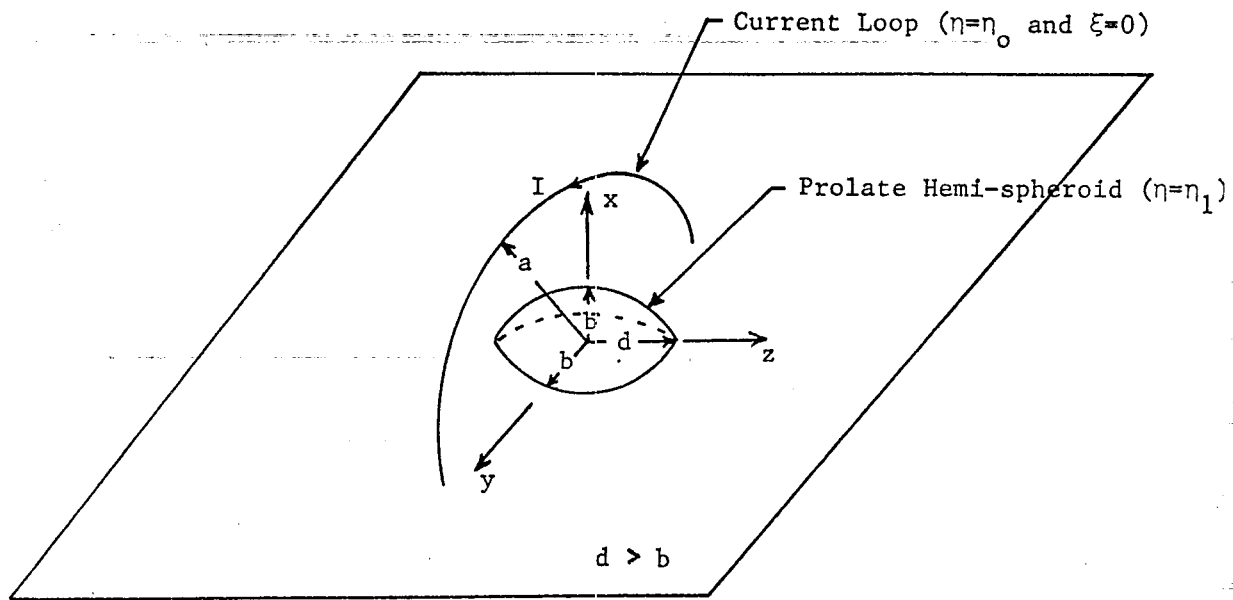


Figure 16. Half Prolate Spheroid Inside a Current Loop

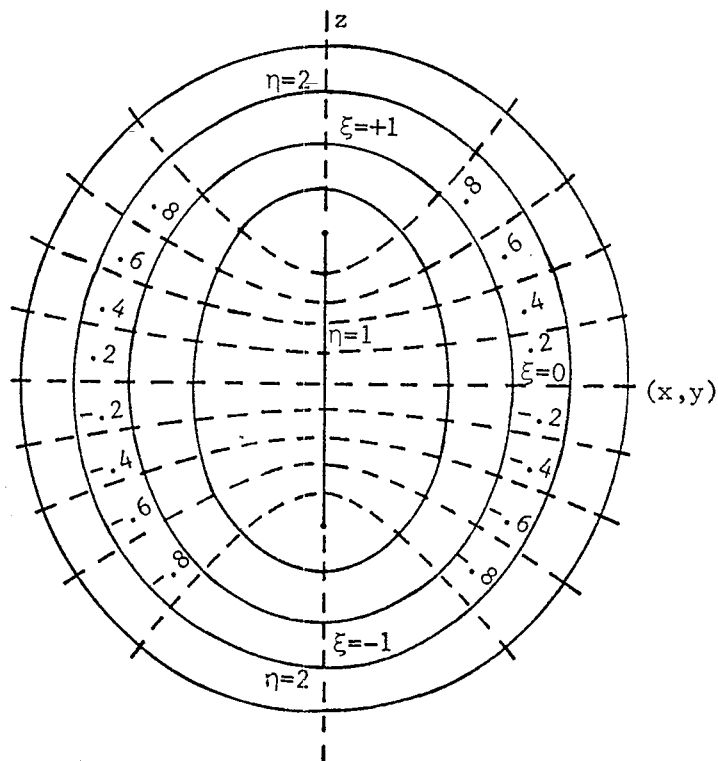


Figure 17. Spheroidal Coordinates

where $a/b = (\eta_0^2 - 1)^{\frac{1}{2}}/(\eta_1^2 - 1)^{\frac{1}{2}}$, and $P_n^1(\xi)$ for $\xi \leq 1$ and $Q_n^1(\eta)$ for $1 \leq \eta < \infty$ are the associated Legendre functions of the first and second kind.

For a fixed finite value of a (a equal to the current loop radius) the limiting cases $b/d \rightarrow 1$ and $b/d \rightarrow 0$ correspond to the problems of a sphere and an infinitely long cylinder.

The plots of Δ_{SO} versus z/d and z/a (z being the symmetrical axis of the prolate hemispheroid and the circular loop) of a spherical test object ($b/d = 1$) and of an infinitely long cylinder ($b/d = 0$), respectively, inside the current loop are shown in figures 18 and 19 with b/a as the parameter. However, the maximum value of Δ_{SO} is shown in figure 20. Note that the maximum deviation Δ_{\max} for $b/a \leq 0.5$, in general, is not at the location $z = 0$ of the nearest distance between loop and object.

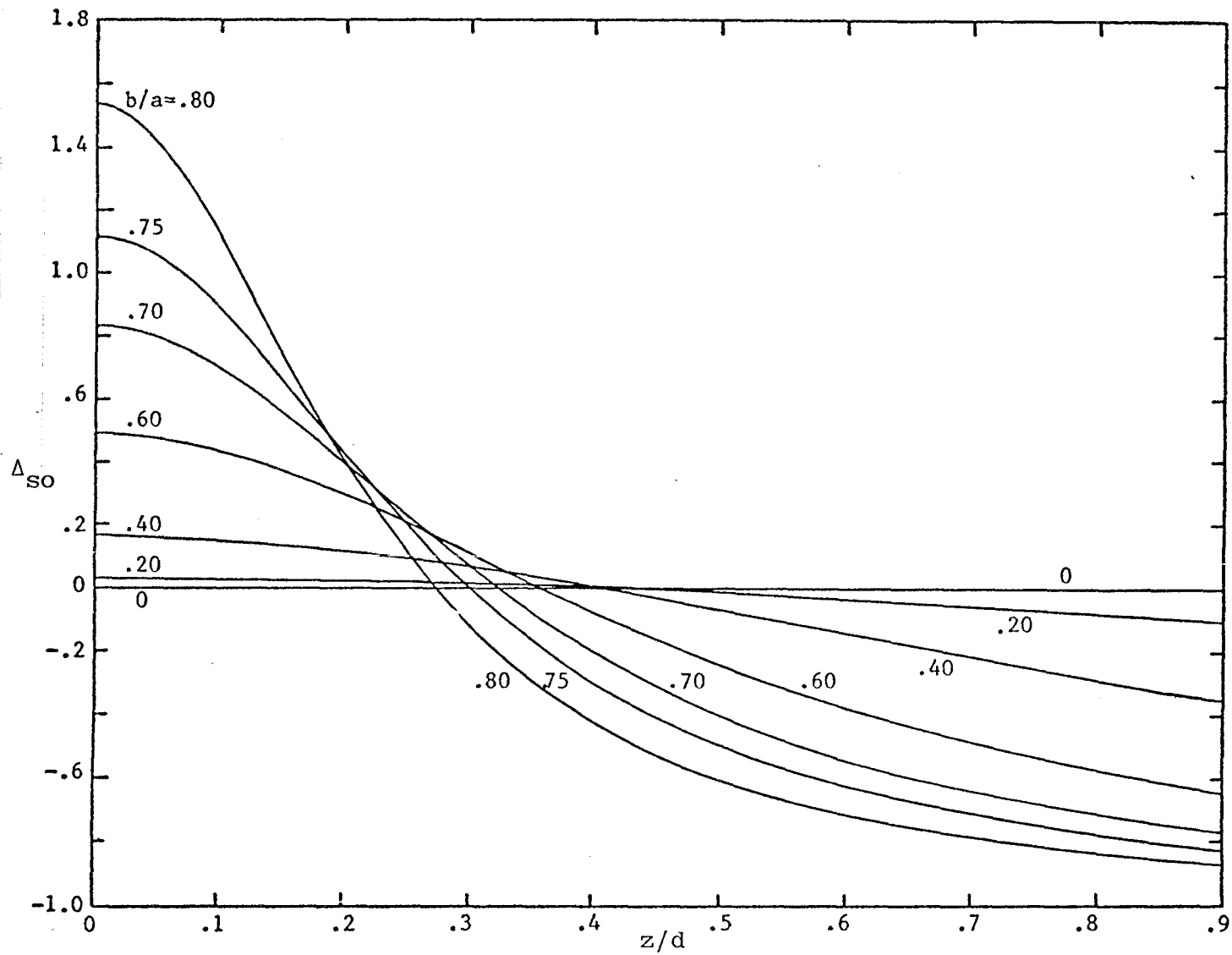


Figure 18. Increment of the Magnetic Field (Equal to Skin Current) on a Conducting Sphere ($d/b = 1$) due to the Simulator/Object Interaction

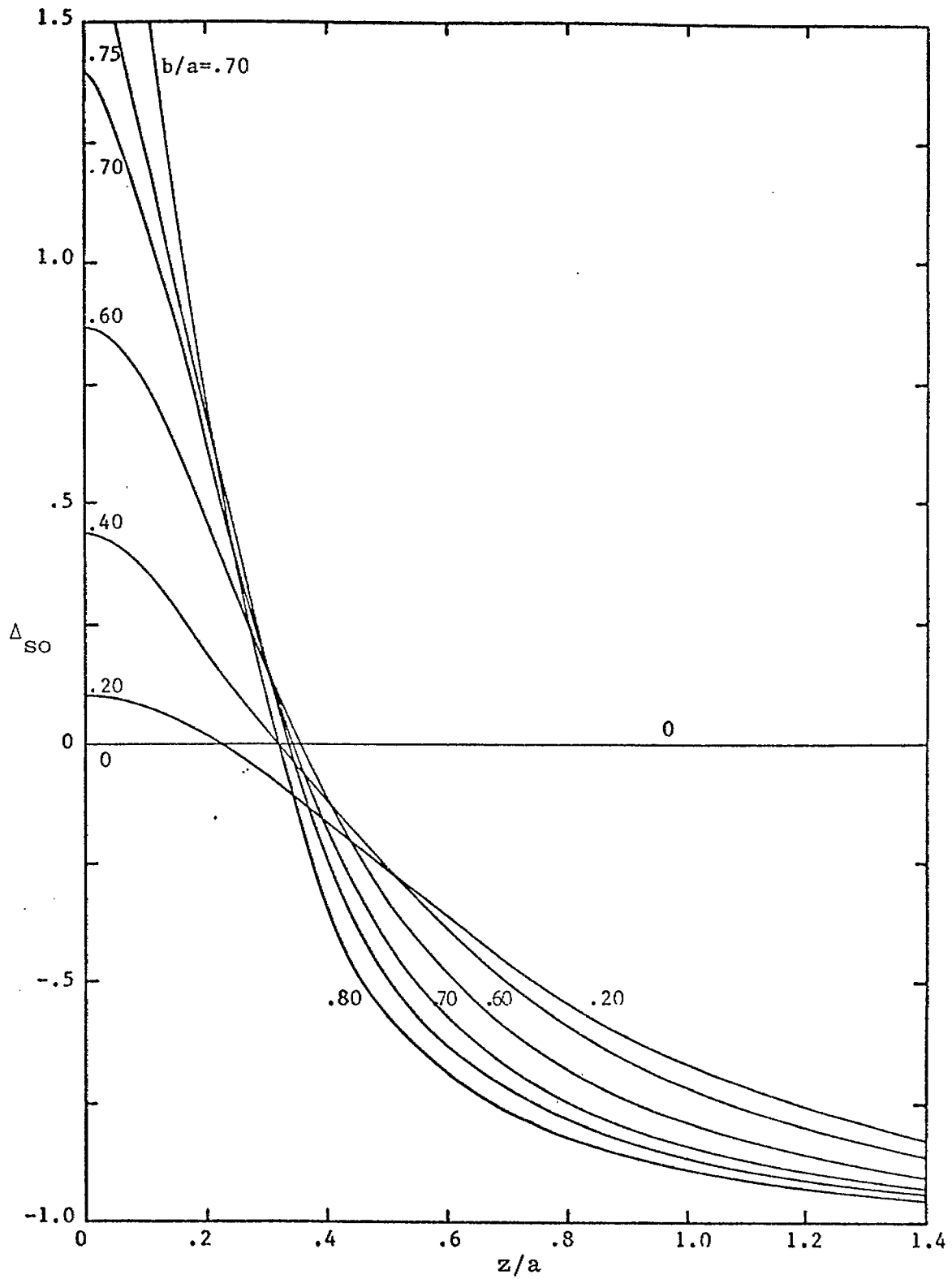


Figure 19. Increment of the Magnetic Field Density Along an Infinitely Long Cylinder ($d/b \rightarrow \infty$) due to the Simulator/Object Interaction

75

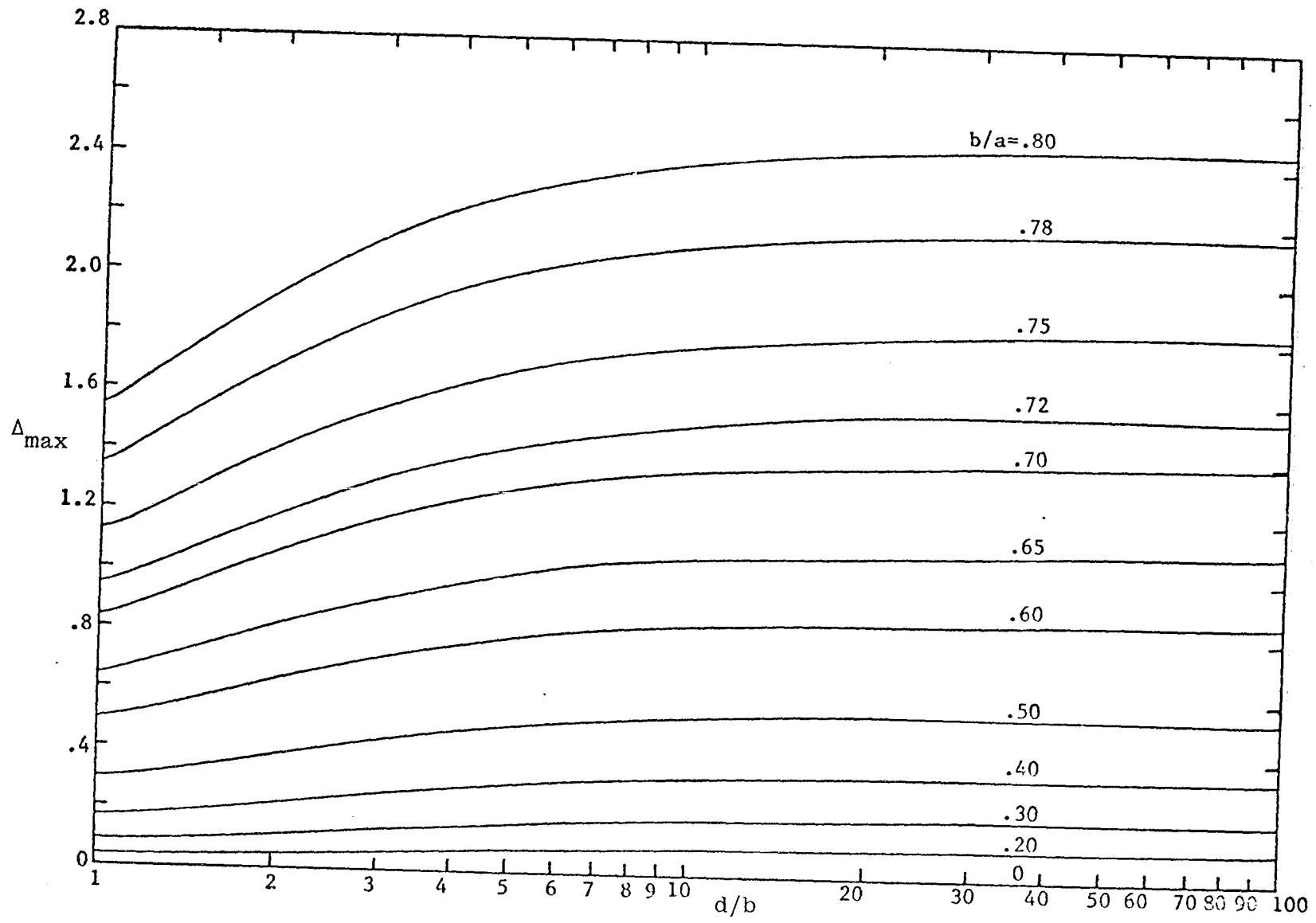


Figure 20. Δ_{\max} is the Maximum Value of Δ over the Spheroid

D. Charged Filament Above an Earthed Slotted Sheet

A filament of charge per unit length denoted by q is situated at a distance d in front of the center of a slit of width $2b$ in the ground plane, as shown in figure 21.

By using the conformal mapping techniques, the complex potential function w can be found to be (ref. 12)

$$w \equiv u + jv = \frac{q}{2\pi\epsilon} \ln \left[\frac{z \pm \sqrt{z^2 - b^2} - j(d \pm \sqrt{d^2 + b^2})}{z \pm \sqrt{z^2 - b^2} + j(d \pm \sqrt{d^2 + b^2})} \right] \quad (74)$$

$z = x + jy =$ complex coordinate

If the imaginary part of the square root in equation (74) is always taken positive, then we use the upper sign (positive sign) for $y \geq 0$ and lower sign for $y < 0$.

The complex electric field $E(z)$ can be obtained by differentiating the potential function with respect to z to give

$$E(z) = E_x - jE_y = \frac{dw}{dz} = \frac{q}{2\pi\epsilon} \frac{2j(1 \pm z/\sqrt{z^2 - b^2})(d \pm \sqrt{d^2 + b^2})}{(z \pm \sqrt{z^2 - b^2})^2 + (d \pm \sqrt{d^2 + b^2})^2} \quad (75)$$

If we let $b = 0$ and $z = 0$, we obtain the short-circuit field at the center of the ground plane. Thus, equation (75) reduces to

$$E_{sc}(0) = j \frac{q}{2\pi\epsilon} \frac{2}{d} = jE_0 \quad (76)$$

$E_0 =$ the short-circuit electric field at the center of the ground plane

12. W. R. Smythe, Static and Dynamic Electricity, Chapter IV, 3rd ed., McGraw-Hill Book Co., New York, 1968.

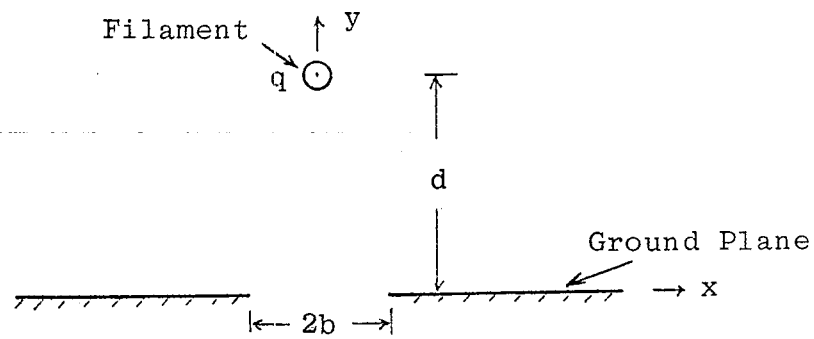


Figure 21. Charged Filament above the Slotted Ground Plane

Inserting E_0 into equation (75) and taking the upper sign only, we rewrite equation (75) by

$$E(z) = jE_0 \frac{(1 + z/\sqrt{z^2 - b^2}) [1 + \sqrt{1 + (b/d)^2}]}{\left[\frac{(z + \sqrt{z^2 - b^2})}{d} \right]^2 + [1 + \sqrt{1 + (b/d)^2}]^2} \quad (77)$$

However, if the slotted ground plane is illuminated by a homogeneous electric field E_0 , the resultant field can be expressed by

$$E_\infty(z) = E(z) \Big|_{\substack{d \rightarrow \infty \\ E_0 = \text{constant}}} = \frac{jE_0}{2} \left(1 + \frac{z}{\sqrt{z^2 - b^2}} \right) \quad (78)$$

Again, we define a parameter Δ_{so} , where Δ_{so} denotes the change of the aperture electric field (equivalent to the fictitious aperture magnetic current) associated with the simulator, to characterize the interaction between the simulator and aperture by

$$\Delta_{so} = \left| \frac{E(z) - E_\infty(z)}{E_\infty(z)} \right|_{\text{aperture}} \quad (79)$$

$$= \left| \frac{(x + j\sqrt{b^2 - x^2})^2 + b^2}{(x + j\sqrt{b^2 - x^2})^2 + (d + \sqrt{d^2 + b^2})^2} \right|_{\substack{\text{at aperture } z=x \\ \text{and } |x| \leq b}}$$

The numerical values of Δ_{so} are given in table 16.

Table 16

DEVIATION OF THE APERTURE ELECTRIC FIELD $10^2 \Delta_{so}$
 DUE TO THE INTERACTION BETWEEN SIMULATOR AND APERTURE

x/b b/d	0.1	0.2	0.3	0.4	0.5	0.6	0.7	0.8	0.9	1.0
0.1	0.050	0.100	0.150	0.199	0.249	0.299	0.348	0.398	0.447	0.496
0.2	0.198	0.396	0.593	0.790	0.985	1.180	1.373	1.564	1.754	1.942
0.3	0.440	0.879	1.316	1.750	2.177	2.600	3.016	3.425	3.826	4.217
0.4	0.770	1.536	2.295	3.043	3.777	4.494	5.193	5.869	6.523	7.152
0.5	1.179	2.349	3.502	4.630	5.725	6.783	7.799	8.767	9.687	10.56
0.6	1.659	3.300	4.907	6.464	7.959	9.382	10.73	11.99	13.16	14.25
0.7	2.201	4.370	6.478	8.499	10.41	12.21	13.87	15.40	16.80	18.08
0.8	2.797	5.542	8.186	10.69	13.03	15.18	17.14	18.91	20.50	21.91
0.9	3.440	6.798	10.000	13.00	15.75	18.23	20.45	22.42	24.15	25.67
1.0	4.122	8.123	11.90	15.38	18.52	21.31	23.75	25.88	27.71	29.29
1.2	5.580	10.93	15.86	20.27	24.10	27.37	30.13	32.44	34.37	35.98
1.4	7.135	13.88	19.93	25.14	29.51	33.10	36.02	38.39	40.31	41.88
1.6	8.757	16.89	23.98	29.88	34.62	38.38	41.34	43.68	45.52	47.00
1.8	10.42	19.93	27.96	34.38	39.36	43.17	46.09	48.33	50.07	51.44
2.0	12.12	22.95	31.80	38.61	43.70	47.48	50.29	52.41	54.03	55.28
3.0	20.71	37.08	48.22	55.37	59.97	63.01	65.07	66.53	67.59	68.38
4.0	29.00	48.77	59.98	66.21	69.83	72.07	73.53	74.52	75.23	75.75
5.0	36.66	57.97	68.21	73.33	76.12	77.77	78.83	79.53	80.03	80.39
10.0	63.99	80.94	85.85	87.80	88.74	89.27	89.59	89.80	89.95	90.05

E. Large Plat Above Slotted Plane

Figure 22 schematically shows a large plate simulator in front of a slotted plane which is maintained at potential $V = -1$. The slit has width $2b$ and is located at a distance h from the top plate. By utilizing the conformal mapping method, the complex coordinate z can be expressed in terms of the complex potential function w by (ref. 12)

$$z - jh = \frac{2h}{\pi} \left[\frac{a^2}{1 - a^2} \tanh\left(\frac{\pi w}{2}\right) + \frac{\pi w}{2} \right]$$

$$z = x + jy \tag{80}$$

$$w(z) = u(x,y) + jv(x,y)$$

where $u(x,y)$ is the stream function and $v(x,y)$ is the potential function.

The above equation can be rewritten in two equations which correspond to the real and imaginary parts of (80):

$$x = \frac{2h}{\pi} \left[\frac{a^2}{1 - a^2} \frac{\sinh(\pi u)}{\cosh(\pi u) + \cos(\pi v)} + \frac{\pi u}{2} \right]$$

$$y - h = \frac{2h}{\pi} \left[\frac{a^2}{1 - a^2} \frac{\sin(\pi v)}{\cosh(\pi u) + \cos(\pi v)} + \frac{\pi v}{2} \right]$$

$$\tag{81}$$

Here, a is a parameter and is related to the slit width $2b$ by

$$b = \frac{2h}{\pi} \left(\tanh^{-1} a + \frac{a}{1 - a^2} \right) \quad \text{for } a < 1 \tag{82}$$

The complex electric field $E(z)$ is obtained by taking the derivative of (80) to give

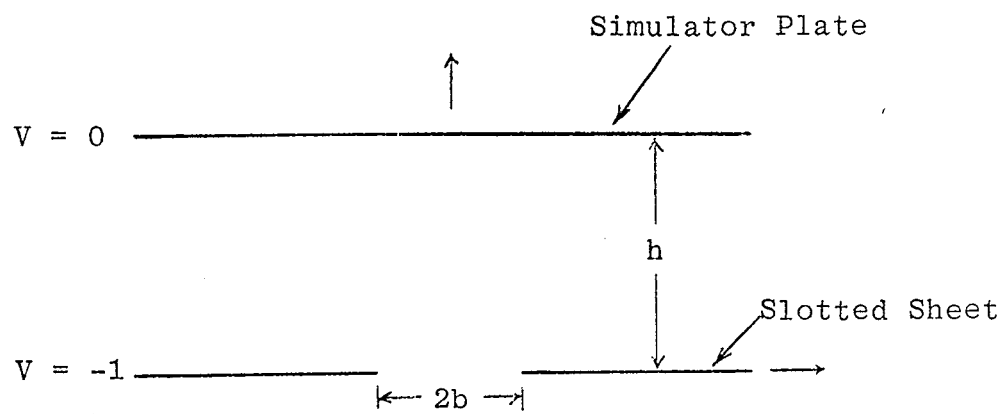


Figure 22. Large Plate in Front of a Slotted Sheet

$$\begin{aligned}
E(z) &= E_y(x,y) + jE_x(x,y) = \frac{dw}{dz} \\
&= \frac{E_0}{1 + \frac{a^2}{1-a^2} \operatorname{sech}^2\left(\frac{\pi w}{2}\right)} \quad (83)
\end{aligned}$$

$$E_0 = \text{short-circuit electric field} = -\frac{1}{h}$$

In the previous subsection, it has been shown that the field of a slotted plane immersed in a uniform electric field E_0 is given by (for the region $y \geq 0$)

$$E_\infty(z) = \frac{E_0}{2} \left(1 + \frac{z}{\sqrt{z^2 - b^2}} \right) \quad (84)$$

Here, imaginary part of the square root is always taken positive, i.e., $\operatorname{Im}(\sqrt{z^2 - b^2}) > 0$

Similarly, the field deviation Δ_{so} at the aperture is defined by

$$\begin{aligned}
\Delta_{so} &= \left| \frac{E(z) - E_\infty(z)}{\bar{E}_\infty(z)} \right|_{\text{aperture}} \\
&= \left| 2 \left[1 + \frac{a^2}{1-a^2} \operatorname{sech}^2\left(\frac{\pi w}{2}\right) \right]^{-1} \left[1 - \frac{jx}{\sqrt{b^2 - x^2}} \right]^{-1} - 1 \right| \quad (85) \\
&\quad \left. \begin{array}{l} \text{at aper-} \\ \text{ture } z=x \\ \text{and} \\ |x| \leq b \end{array} \right\}
\end{aligned}$$

Letting $z = x$, the complex potential w is determined from (80) and (82) which reduce to

$$\begin{aligned}
x - jh &= \frac{2h}{\pi} \left[\frac{a^2}{1-a^2} \tanh\left(\frac{\pi w}{2}\right) + \frac{\pi w}{2} \right] \\
b &= \frac{2h}{\pi} \left(\tanh^{-1} a + \frac{a}{1-a^2} \right) \quad \text{for } a < 1 \quad (86)
\end{aligned}$$

It is of interest to examine the field function (83) by taking the limit $h \rightarrow \infty$ and (83) should be reduced to (84). As one can see, if the top plate $V = 0$ of figure 22 approaches to infinity, the field near the aperture is small and the potential near the aperture will be very close to the potential of the slotted plane $V = -1$. Then we can express the potential function w as

$$w \approx -j + \delta, \quad \delta \ll 1 \quad (87)$$

where δ denotes the stream function near the aperture and δ is small.

As $h \rightarrow \infty$, from (82) we find the parameter a to be

$$a \approx \frac{\pi}{4} \frac{b}{h} \quad (88)$$

By utilizing expressions (87) and (88), from (80), we obtain

$$\delta^2 - \frac{z}{h} \delta + \frac{b^2}{4h^2} = 0 \quad (89)$$

or

$$\delta = \frac{z + \sqrt{z^2 - b^2}}{2h}$$

Note that the positive sign in front of the square root is used here. Thus, the denominator of the field function (83) is reduced to

$$\begin{aligned} D &= 1 + \frac{a^2}{1 - a^2} \operatorname{sech}^2 \left(\frac{\pi w}{2} \right) \approx 1 + \left(\frac{\pi \delta}{2} \right)^2 \left(\frac{z}{h\delta} - 1 \right) \left[j \operatorname{csch} \left(\frac{\pi \delta}{2} \right) \right]^2 \\ &= 2 - \frac{z}{h\delta} = 2 \left[\frac{\sqrt{z^2 - b^2}}{z + \sqrt{z^2 - b^2}} \right] \end{aligned} \quad (90)$$

Inserting (90) into (83), we have

$$E \Big|_{\substack{h \rightarrow \infty \\ E_0 = \text{constant}}} = \frac{E_0}{2} \left[1 + \frac{z}{\sqrt{z^2 - b^2}} \right] = E_\infty \quad (91)$$

The field deviation Δ_{s0} in the aperture due to the interaction of simulator plate and aperture is tabulated in table 17.

Table 17

DEVIATION OF THE APERTURE ELECTRIC FIELD $10^2 \Delta_{so}$
 DUE TO THE INTERACTION BETWEEN SIMULATOR AND APERTURE

x/b b/d	0.0	0.1	0.2	0.3	0.4	0.5	0.6	0.7	0.8	0.9
0.2	0.808	0.847	0.845	0.835	0.819	0.800	0.784	0.788	0.830	0.833
0.3	1.791	1.810	1.811	1.809	1.804	1.798	1.794	1.793	1.788	1.795
0.4	3.122	3.132	1.132	3.128	3.121	3.113	3.103	3.093	3.053	3.057
0.5	4.757	4.758	4.753	4.743	4.727	4.707	4.682	4.652	4.595	4.570
0.6	6.641	6.637	6.625	6.603	6.571	6.530	6.481	6.421	6.334	6.270
0.7	8.729	8.718	8.695	8.656	8.601	8.531	8.446	8.330	8.215	8.099
0.8	10.97	10.95	10.92	10.86	10.77	10.66	10.53	10.36	10.19	10.01
0.9	13.32	13.30	13.25	13.16	13.03	12.88	12.69	12.46	12.21	11.95
1.0	15.74	15.72	15.64	15.52	15.35	15.14	14.89	14.58	14.25	13.90
1.1	18.20	18.17	18.07	17.92	17.70	17.42	17.10	16.71	16.29	15.83
1.2	20.67	20.63	20.51	20.32	20.05	19.70	19.29	18.81	18.29	17.73

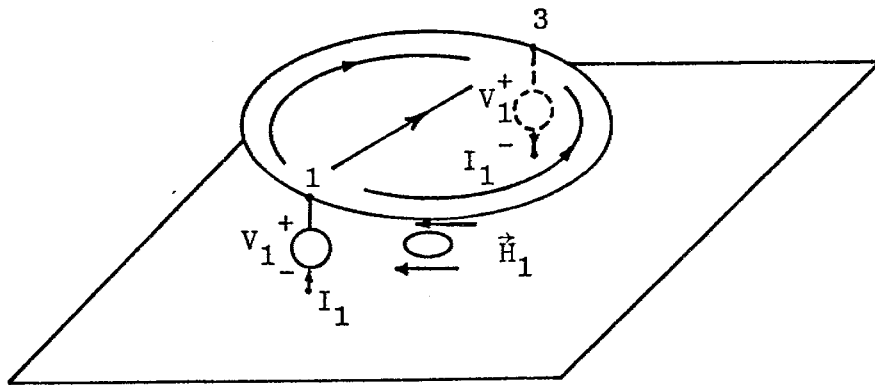
V. Summary

Analysis of other important geometries pertinent to FINES has appeared in the literature and is not included in this report. Those geometries are a circular disk (ref. 13), a spherical cap (ref. 14) above the ground plane for the E-field simulators, the multiloops wound on a hemi-cylindrical surface (ref. 15), and a hemispherical surface (ref. 7) above the ground plane for the H-field simulators. For simulator/object interaction problems, one of the important generic studies concerning a circular disk in front of a circular aperture in the ground plane has been solved by reference 16, and a cylindrical post sited on the ground plane below a large simulator plate can be found in references 17, 18, and 19 where the static solution is of interest. Solutions to

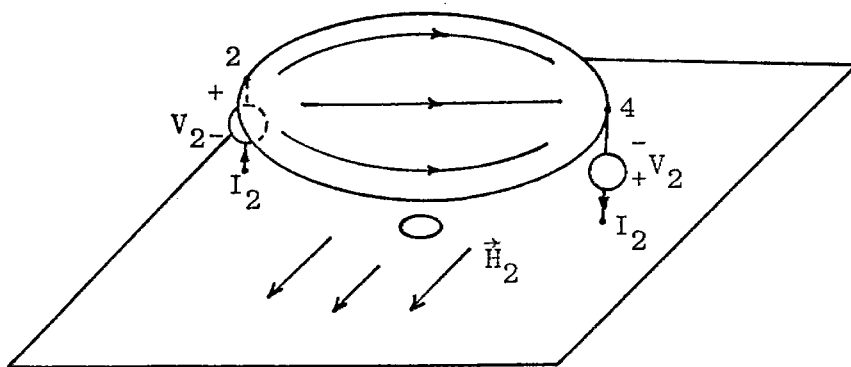
-
13. C. E. Baum, "The Circular Parallel-Plate Dipole," Sensor and Simulation Note 80, March 1969.
 14. C. E. Baum, "The Single-Gap Hollow Spherical Dipole in Non-Conducting Media," Sensor and Simulation Note 91, July 1969.
 15. C. E. Baum, "Some Considerations for Electrically-Small Multi-Turn Cylindrical Loops," Sensor and Simulation Note 55, May 31, 1967.
 16. F. C. Yang and L. Marin, "An Electrical-Field-Penetration Simulator for Apertures," Sensor and Simulation Note (to be published).
 17. Clayborn D. Taylor, George A. Steigerwald, "On the Pulse Excitation of a Cylinder in a Parallel Plate Waveguide," Sensor and Simulation Note 99, March 1970.
 18. R. W. Latham and K.S.H. Lee, "Electromagnetic Interaction Between a Cylindrical Post and a Two-Parallel-Plate Simulator," Sensor and Simulation Note 111, July 1970.
 19. Lennart Marin, "A Cylindrical Post Above a Perfectly Conducting Plate, I (Static Case)," Sensor and Simulation Note 134, July 1971.

these problems are considerably difficult to obtain. Future studies are suggested to choose one or two configurations from the above canonical problems for detailed consideration.

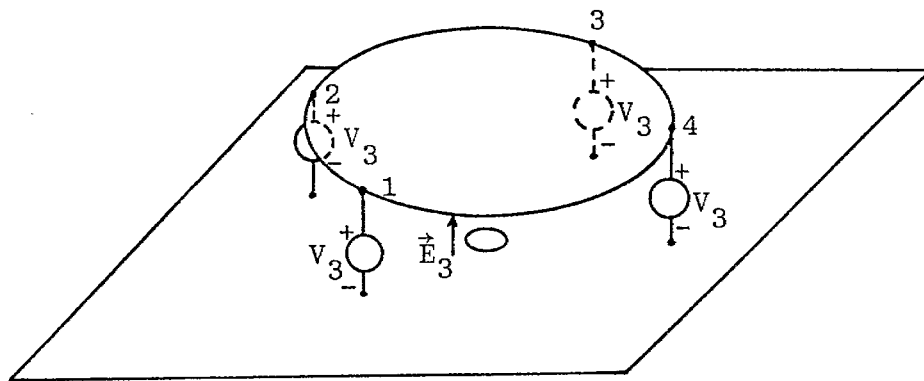
One of the simple driving networks for single- and multiple-field-component FINES can be shown schematically in figure 23 in which a circular disk simulator is driven by generators spaced in quadrants along its circumference. If the simulator is driven by a source pair of opposite polarities, as shown in figure 23(a) of the source pair 1 and 3 and also in figure 23(b) of the source pair 2 and 4, the simulator becomes the H-field type. From the directions of current flow as indicated in figures 23(a) and (b), the fields \vec{H}_1 and \vec{H}_2 generated by the simulator are orthogonal. However, if all the sources are identical (including the connecting cables between the source and simulator) and are in the same polarity, as shown in figure 23(c), the simulator becomes the E-field type. The possible network in feeding this simulator is shown in figure 24. Here, two independent current sources are used to drive the transformer pairs A and C, and B and D to generate the magnetic fields \vec{H}_1 and \vec{H}_2 , respectively. A single voltage source is connected in such a way to generate only the electric field. Note that the transformer pair A and C is not coupled to the transformer pair B and D. To achieve mutual coupling between A and C a bifilar (or trifilar or quadrafilar) winding is used, and similarly for B and D. The details of such a design need study.



a. H-field Type



b. H-field Type



c. E-field Type

Figure 23. Simulator with the Sources Spaced in Quadrants Along the Disk's Rim

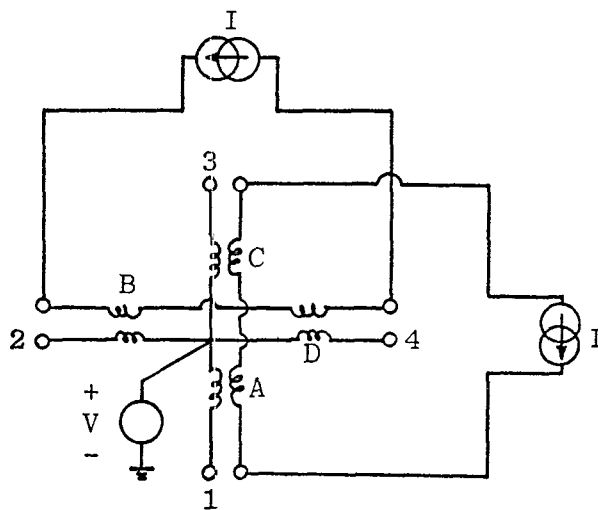


Figure 24. Feeding Network for the Multiple-Field-Component FINES

Another possible combined fields simulator, as shown in figure 25, is the combination of an H-field simulator consisting of some current loops such as the Helmholtz coils and an E-field simulator such as a circular disk above the ground plane. It is desired that the E-field simulator be driven by a voltage source and the H-field be driven by a current source. An exact analytical solution to the combined structures by solving a rather complicated boundary-value problem may be difficult to obtain. However, by symmetry in design, we are able to keep the coupling between the multiple field components negligibly small. Hence, the problem of a composite structure can be resolved into two rather simple canonical problems where the analytical solutions are possible. Other engineering problems in the design of a FINES, such as the choices of the sources and the matching networks which will directly affect the desired waveform and power efficiency, should also be included for future consideration.

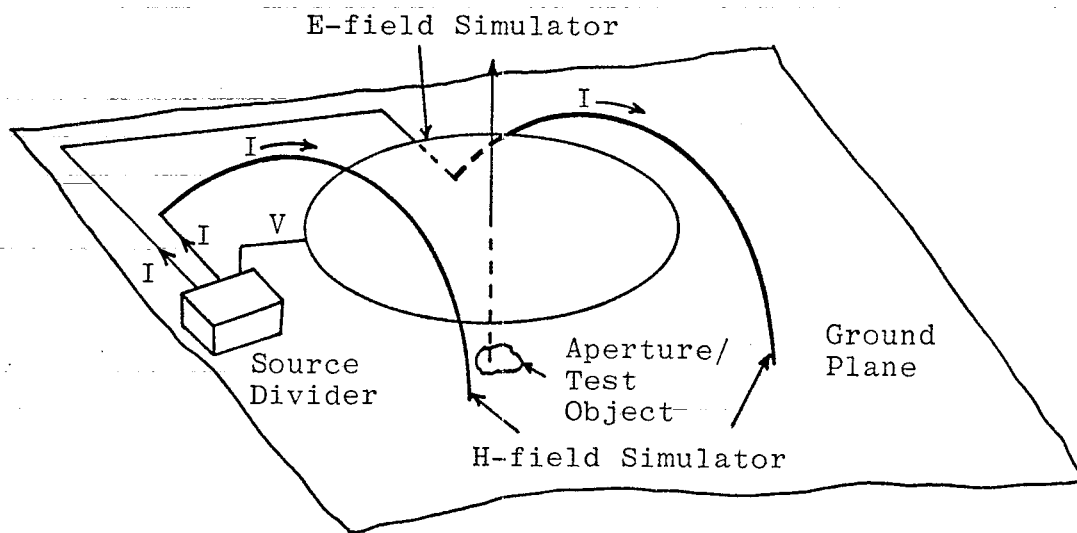


Figure 25. Combined Field Simulator

References

1. C. E. Baum, "EMP Simulators for Various Types of Nuclear EMP Environments: An Interim Categorization," Sensor and Simulation Note 151, 13 July 1972, AFWL. Also adapted for Special Joint Issue on the Nuclear Electromagnetic Pulse, IEEE Trans. Antennas and Propagation, January 1978, and IEEE Trans. Electromagnetic Compatibility, February 1978.
2. C. E. Baum, E. L. Breen, J. C. Giles, J. O'Neil, and G. D. Sower, "Sensors for Electromagnetic Pulse Measurement Both Inside and Away from Nuclear Source Regions," Special Joint Issue on Nuclear Electromagnetic Pulse, IEEE Trans. Antennas and Propagation, January 1978, and IEEE Trans. Electromagnetic Compatibility, February 1978.
3. C. E. Baum, D. V. Giri, and R. D. Gonzalez, "Electromagnetic Field Distribution of the TEM Mode in a Symmetric Two-Parallel-Plate Transmission Line," Sensor and Simulation Note 219, 1 April 1976.
4. Tom K. Liu, "Impedances and Field Distribution of Curved Parallel-Plate Transmission-Line Simulators," Sensor and Simulation Note 170, February 1973.
5. K. D. Granzow, "Homogeneity of the Magnetic Field of a Helmholtz Coil," SCR-193, Sandia Corporation Monograph, July 1960.
6. J. C. Maxwell, Electricity and Magnetism, Chapter XV, Volume Two, Dover Publications, Inc., New York, 1954.
7. J. E. Everett and J. E. Osemeikhian, "Spherical Coils for Uniform Magnetic Fields," J. Sci. Instrum., Vol. 43, pp. 470-474, 1966.
8. W. R. Smythe, Static and Dynamic Electricity, Chapter VIII, 3rd ed., McGraw-Hill Book Co., New York, 1968.
9. R. W. Latham, "Interaction Between a Cylindrical Test Body and a Parallel Plate Simulator," Sensor and Simulation Note 55, May 1968.
10. Soon K. Cho and Chiao-Min Chu, "A Parametric Study of a Circular Cylinder within Two Parallel Plates of Finite Width," Sensor and Simulation Note 174, January 1973.
11. A. D. Varvatsis and M. I. Sancer, "Low-Frequency Magnetic Field Interaction of a Half Toroid Simulator with a Perfectly Conducting Half Prolate Spheroid," Sensor and Simulation Note 131, June 1971.

12. W. R. Symthe, Static and Dynamic Electricity, Chapter IV, 3rd ed., McGraw-Hill Book Co., New York, 1968.
13. C. E. Baum, "The Circular Parallel-Plate Dipole," Sensor and Simulation Note 80, March 1969.
14. C. E. Baum, "The Single-Gap Hollow Spherical Dipole in Non-Conducting Media," Sensor and Simulation Note 91, July 1969.
15. C. E. Baum, "Some Considerations for Electrically-Small Multi-Turn Cylindrical Loops," Sensor and Simulation Note 55, May 31, 1967
16. F. C. Yang and L. Marin, "An Electrical-Field-Penetration Simulator for Apertures," Sensor and Simulation Note (to be published).
17. Clayborn D. Taylor, George A. Steigerwald, "On the Pulse Excitation of a Cylinder in a Parallel Plate Waveguide," Sensor and Simulation Note 99, March 1970.
18. R. W. Latham and K.S.H. Lee, "Electromagnetic Interaction Between a Cylindrical Post and a Two-Parallel-Plate Simulator," Sensor and Simulation Note 111, July 1970.
19. Lennart Marin, "A Cylindrical Post Above a Perfectly Conducting Plate, I (Static Case)," Sensor and Simulation Note 134, July 1971.

Acknowledgment

The authors wish to thank Drs. J. S. Yu, K.S.H. Lee and L. Marin of Dikewood Industries, Inc. for their technical discussions, and Dr. J. Chen of Dikewood for his assistance on the computer programming.